Gas Metal Arc Welding of Magnesium Alloys: Oxide Films, High Crowns, and Fingers

Sound welds can be made but precautions need to be taken against these defects, whose mechanisms of formation are established and methods of mitigation demonstrated

BY X. CHAI, Y. K. YANG, B. E. CARLSON, AND S. KOU

ABSTRACT

The use of Mg alloys for vehicle weight reduction has been increasing rapidly worldwide. Gas metal arc welding (GMAW) has the potential for mass-production welding of Mg alloys. Recently, the University of Wisconsin demonstrated in bead-on-plate GMAW of Mg alloys that: 1) the issue of severe spatter, which has long delayed the use of GMAW for Mg alloys, can be eliminated by using controlled short circuiting (CSC), and 2) the issue of severe hydrogen porosity can be eliminated by removing $Mg(OH)_2$, which forms on the welding wire surface over time. The present study aimed at actual butt and lap joint welding of Mg alloys by CSC-GMAW. The most widely used wrought Mg alloy AZ31 Mg (~Mg-3Al-1Zn-0.2Mn) was welded by CSC-GMAW. Sound welds were made without spatter and hydrogen porosity, with butt joint welds approaching 100% of the base-metal strength. However, three new significant issues were found to occur easily and degrade the weld quality significantly: 1) formation of oxide films inside butt joint welds, 2) formation of high crowns on butt joint welds, and 3) formation of fingers from lap joint welds. These three new issues, like the issues of spatter and porosity investigated previously, were caused mainly by the unusual physical and chemical properties of Mg, rather than the welding process itself. These properties include the low liquid density, low solid deformability, low liquid fluidity, and high oxygen affinity of Mg. The mechanisms of their formation were established, and the methods for their elimination or reduction were demonstrated.

KEYWORDS

• Mg Alloys • Gas Metal Arc Welding (GMAW) • Controlled Short Circuiting (CSC) • Butt Joint Welds • Lap Joint Welds

Introduction

The automotive industry has been using lighter structural materials including magnesium alloys (Refs. 1, 2) to reduce vehicle weight, fuel consumption, and emissions. Being one-third lighter than aluminum (Al), magnesium (Mg) is the lightest metallic structural material with excellent specific strength (Ref. 3). Due to the rapidly increasing use of Mg alloys (Refs. 1–3), research interest in Mg welding has grown rapidly as can be seen in reviews on recent Mg welding research (Refs. 4–7). Spatter has long delayed the use of gas metal arc welding (GMAW) for Mg alloys. Spatter is the "metal particles expelled during fusion welding that do not form a part of the weld" (Ref. 8). It is caused by the expelling of filler metal droplets from the arc during welding. Severe spattering can result in a messy weld irregular in shape, with significant variations in the weld width and penetration depth. Fifty percent or more loss of the Mg filler metal by spattering has been reported (Refs. 5, 9).

Lockwood (Ref. 10) pioneered the GMAW of Mg alloys. He found that spray transfer at high welding currents produced too much heat for welding thin Mg sheets, and globular transfer was unstable and caused spattering. So, he used short-circuit transfer to weld sheets from 1.0 to 3.2 mm (0.04–0.125 in.). The resultant welds showed rather high crowns. Lockwood (Ref. 11) also tried pulsed-arc welding at intermediate currents, where one small droplet was transferred per pulse. Rethmeier et al. (Ref. 12) welded AZ31 Mg and AZ61 Mg alloys by short-circuiting GMAW, and welds with high crowns were shown.

Mg alloys have been welded by gas tungsten arc welding (GTAW) (Ref. 13), laser beam welding (LBW) (Refs. 6, 14), electron beam welding (EBW) (Ref. 15), friction stir welding (FSW) (Ref. 16), and double-sided plasma arc welding (DSPAW) (Ref. 17). Gas tungsten arc welding is slow, LBW and

X. CHAI is a graduate student, Y. K. YANG was a postdoc, and S. KOU is a professor with the Department of Materials Science and Engineering, the University of Wisconsin, Madison, Wis. B. E. CARLSON is with the Manufacturing System Lab, General Motors Research and Development Center, Warren, Mich.

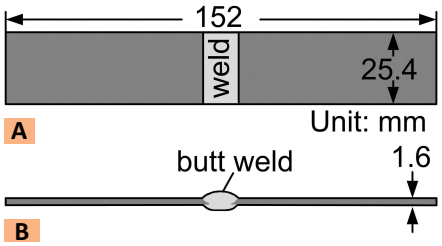

Fig. 1 — Specimen for tensile testing in the transverse direction of a butt joint weld. A — Top view; B — side view.

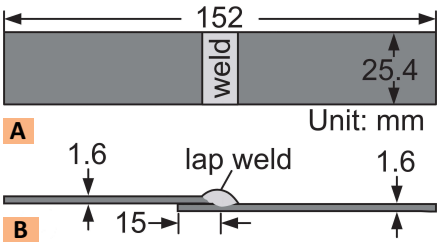

Fig. 2 — Specimen for tensile testing in the transverse direction of a lap weld. A — Top view; B — side view.

EBW are not readily available, and DSPAW can be inconvenient. Friction stir welding requires rigid clamping and the use of an anvil, and can be complicated for making fillet welds. Gas metal arc welding, if it can be used for Mg alloys, is readily available, inexpensive and easy to use, and it combines good weld quality, high production rate, and easy automation.

Recently, the University of Wisconsin demonstrated the elimination of spatter in GMAW of Mg alloys by using controlled short circuiting (CSC) (Ref. 18). In CSC-GMAW, a process controller coordinates the feeding and speed of the wire electrode with the level of welding current delivered by the power source (Ref. 19). The controller monitors the voltage between the electrode and the workpiece to determine if the welding process is in the arc phase or the short-circuiting phase at any given time. The controller clears the short by retracting the wire to the preset arc length level. Once the arc is established again, the controller begins feeding the wire toward the weld pool, and the cycle repeats. CSC-GMAW was originally developed and called "CSC-MIG" by Miller Electric Manufacturing Co. and subsequently manufactured by Jetline Engineering, Irvine, Calif. This was the first application of CSC-GMAW to Mg alloys.

The mechanism of spatter in conventional GMAW of Mg alloys was established by examining the metal transfer by high-speed video recording at 4000 frames/s and analyzing the waveforms of current and voltage recorded during welding (Ref. 18). Essentially, the low Mg density makes the Mg welding wire both fast melting and difficult to detach by gravity. The excessively large globule finally touches the weld pool to short circuit. This causes a sudden current surge, which in turn causes the arc to suddenly expand during reinitiation and expel the large globule as severe spatter. In CSC-GMAW, however, the current is always under tight control, and there is no current surge to cause spatter.

Severe hydrogen porosity, though not reported previously in GMAW of Mg alloys, was observed in both conventional GMAW and CSC-GMAW (Ref. 18). It was demonstrated that porosity can be eliminated by cleaning the Mg welding wire surface with sandpaper or baking it in air at 380°C for 11 min before welding. The mechanism of porosity formation in Mg GMAW was also established by using X-ray diffraction to identify the presence of $Mg(OH)_2$ on the welding wire that caused porosity and by using the solubility curve of H in Mg. Essentially, with its large surface area per unit volume, a welding wire covered with $Mg(OH)_2$ can carry a significant amount of $Mg(OH)_2$ into the arc, where it decomposes by $Mg(OH)_2 \rightarrow MgO + H_2O$. The H_2O further decomposes to hydrogen to dissolve in Mg(L) as H. Since Mg(S) can dissolve much less H than Mg(L), it rejects H to form a H-rich liquid layer at the solidification front, where the reaction $2H \rightarrow H_2(g)$ can occur and form hydrogen bubbles. The low Mg density slows down the rise of the bubbles to escape from the weld pool.

The purpose of the present study was to actually butt and lap joint weld Mg-alloy sheets together by CSC-GMAW. In the previous study (Ref. 18), bead-on-plate welding was used to demonstrate the elimination of spatter and hydrogen porosity from Mg welds by CSC-GMAW. As will be shown, other defects can form in actual butt and lap joint welding of Mg alloys even though spatter and hydrogen porosity can be eliminated.

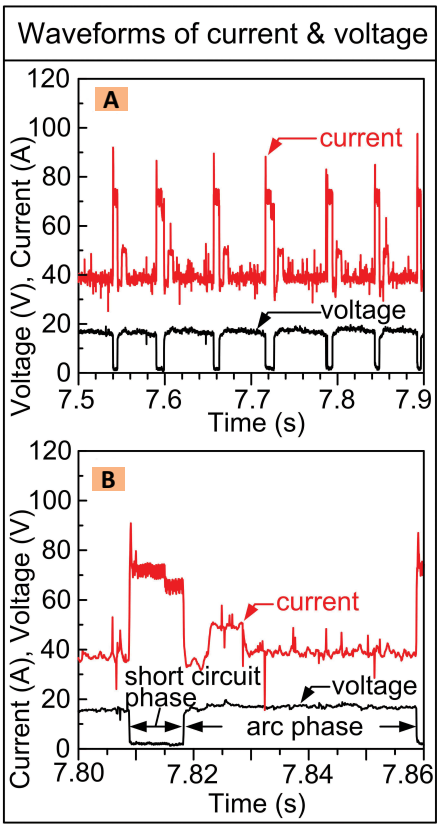

Fig. 3 — Waveforms of welding current and voltage recorded during welding of weld G011. A — Overview; B — enlarged.

Experimental Procedure

Materials

The workpiece was AZ31B-H24 Mg (~Mg-3Al-1Zn-0.2Mn) sheets 203 mm long (rolling direction), 76 mm wide, and 1.6 mm thick (8 by 3 by 1/16 in.). They were cut from a larger sheet by shearing, which is common practice for preparing metal sheets for welding. The filler metal was AZ61A Mg (Mg-6Al-1Zn-0.33Mn) 1.2 mm in diameter. The standard welding grade Ar (99.95% purity) was used as the shielding gas.

All sheets were welded in the length direction (203 mm), that is, the rolling direction. Prior to welding, the surfaces of the workpiece were degreased with acetone, cleaned with a stainless steel brush to remove surface oxides, and then cleaned, including the edges, with acetone again. The filler metal,

on the other hand, was cleaned with acetone, 240-grit sandpaper followed by 600-grit sandpaper, and then acetone again (Ref. 18).

Butt Joint Welding

The welding system consisted of a Miller Electric Invision 456P as the power source and a Jetline Engineering CSC-MIG weld process controller. The welding position was flat and the welding gun was vertical with a distance of 13 mm (½ in.) between the contact tip and workpiece. Tables 1 and 2 show examples of the values that can be assigned to the parameters defining the welding current and wire feed speed, respectively (Ref. 18). Tables 3 and 4 show the values assigned to the parameters defining the welding current and wire feed rate for butt joint welds made with a root opening below 1 mm (0, 0.5, and 0.75 mm). Tables 5 and 6 show similar values for butt joint welds made with a root opening of 1 or 1.2 mm.

Table 1 — Parameters Related to Welding Current in CSC-GMAW

		Current (A)	Times (ms)
A	Start	150	4.0
R	Mid	310	20.0
C	End	110	
S		Current (A)	Times (ms)
H	Start	90	4.0
O	Mid	110	8.0
R	End	90	
T			

Rise (A/ms) 500
Fall (A/ms) 500

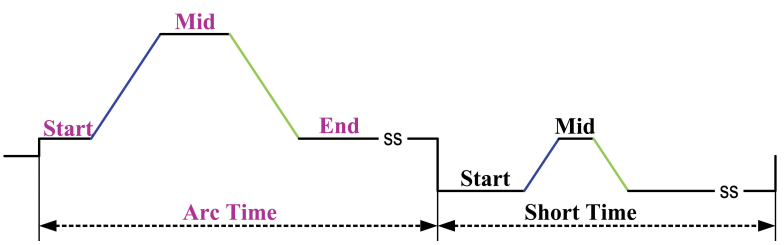

ms: milliseconds.

Table 2 — Parameters Related to Wire Feed Speed in CSC-GMAW

18.5	Down WFS (MPM) (Increasing the down WFS will decrease the deposition rate)
0.0	Delay before wire down (ms) (Pause time at arc length)
15.0	Up 1 WFS (MPM) (Retract WFS until the short is cleared)
0.0	Delay before wire up (ms) (Pause time in the short) (Wire stopped)
15.0	Up 2 WFS (MPM) (Retract WFS after the short is cleared until the arc length is met)
0.0	Arc length (mm) (The distance that the wire will retract after the short has cleared)
0.8	Penetration delay (ms) (After a short is detected, the wire continues forward until time out)

WFS: wire feeding speed; MPM: meters per min; ms: milliseconds.

As shown in Tables 7 and 8, the travel speeds were 7.6, 11.0, or 14.4 mm/s (18, 26, or 34 in./min). The groove in the steel backing plate was 0.44, 0.65, or 1.18 mm deep. The transverse cross-sections of the resultant welds were examined by optical microscopy.

Lap Joint Welding

The upper sheet was 76 mm wide and 203 mm long (rolling direction), and the lower sheet 92 mm (3⅝ in.) wide and 203 mm long (rolling direction), both 1.6 mm thick. The overlapping was 15.88 mm (⅝ in.). A mild steel plate with a groove 1.0 mm (0.04 in.) deep and 9.5 mm (0.375 in.) wide was used as a backing plate for welding. All welds were made with the joint directly on top of the groove except for weld #031, which was made on the same backing plate without a groove. The welding position was flat and the torch was either vertical or tilted 10 deg to a point toward the upper sheet, with a distance of 15.88 mm between the contact tip and upper sheet. The lateral position of the welding wire tip varied from slightly within the upper sheet to slightly within the lower sheet. The travel speed was either 7.62 or 10.2 mm/s (18 or 24 in./min). Similar to butt joint welding, lap joint welding was conducted along the rolling direction of AZ31 Mg.

In both butt and lap joint welding, the waveforms of the welding current and voltage were recorded using a computer data-acquisition system together with the software *LabView*. The data-sampling rate for each signal was 15,000 Hz. The average power input was determined by integration of the product of current and voltage and division over the whole welding time.

Mechanical Testing

Tensile testing of the resultant

Table 3 — Welding Current Settings for Butt Joint Welding with an Opening < 1 mm

						Current					
		Arc Time						Short Circuit Time			
Start		Mid		End		Start		Mid		End	
Current (A)	Time (ms)	Current (A)	Time (ms)	Current (A)	Time (ms)	Current (A)	Time (ms)	Current (A)	Time (ms)	Current (A)	Time (ms)
50	2.0	60	7.0	50	n/a	70	2.0	70	2.5	64	n/a

Rise Rate of Current (A/ms): 250; Fall Rate of Current (A/ms): 250

ms: milliseconds.

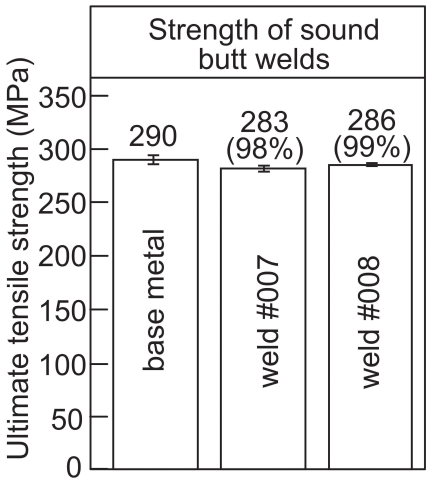

Fig. 4 — Tensile test results of sound butt joint welds.

welds was conducted. The purpose was to understand the effect of various defects on welds instead of documenting the mechanical properties of Mg welds. Specimens for tensile testing were prepared in the transverse direction of the welds, that is, normal to the rolling direction.

Figures 1 and 2 show sketches of the butt-joint and lap-joint weld specimens, respectively. The gauge length for all the tensile specimens was 80 mm, and all tensile tests were conducted with weld crown on. For the purpose of comparison, specimens of 152 by 25.4 by 1.6 mm were also prepared from the same AZ31B-H24 Mg sheets used for welding, with the length direction (152 mm) normal to the rolling direction. Thus, the weld specimens and base-metal specimens were both pulled normal to the rolling direction. For all the tests conducted, the tensile stress was based on the cross-sectional area of 25.4 by 1.6 mm and the value for each weld was the average value of three or more tensile test specimens cut from the same weld. A MTS model Sintech 10/GL tensile testing machine was used. The crosshead movement speed was set at 5 mm/min (0.2 in./min).

Result and Discussion

Butt Joint Welding

Tables 7 and 8 summarize the welding conditions and tensile testing results of the butt joint welds made in the present study. Examples of the

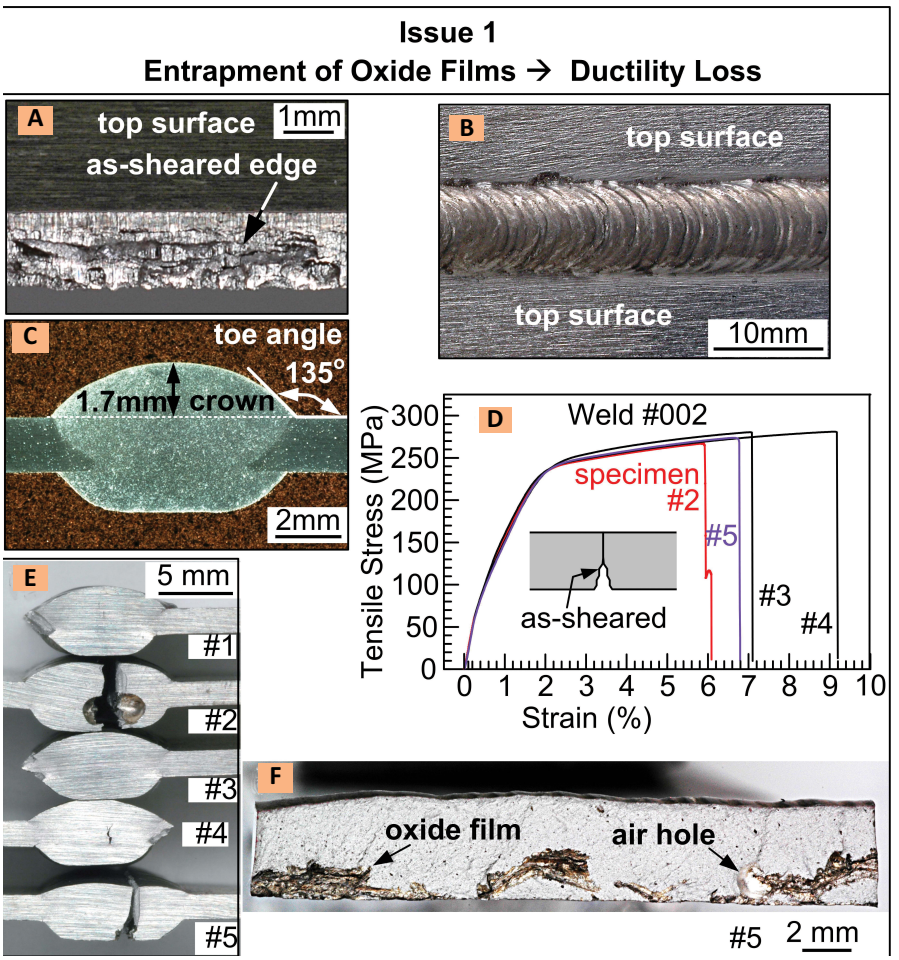

Fig. 5 — Entrapment of oxide films in weld 002. A — Rough edge caused by shearing; B — top view of weld; C — transverse cross section of weld; D — tensile test curves; E — side views of tensile tested specimens; F — fracture surface of specimen 5 showing entrapped oxide films and air holes.

Table 4 — Wire-Speed Settings for Butt Joint Welding with a Root Opening < 1 mm

Wire Speed						
Down		Up 1		Up 2		
Wire Down Speed (MPM)	Delay before Wire Down (ms)	Wire Up 1 Speed (MPM)	Delay before Wire Up (ms)	Wire Up 2 Speed (MPM)	Arc Length (mm)	Penetration Delay (ms)
6.8	4	6.8	6	6.8	0.0	0.8

MPM: meters per min, ms: milliseconds.

waveforms of the welding current and voltage are shown in Fig. 3, which were recorded during the CSC-GMAW of weld G011.

The current settings are shown in Tables 3 and 5, the wire-speed settings in Tables 4 and 6, and the welding conditions in Tables 7 and 8. The welds were free of spatter as will be shown subsequently. They were also free of hydrogen porosity. Hydrogen pores, when they are present, often reach the weld top surface as open holes (Ref. 18). This confirms the previous study based on bead-on-plate welding that CSC can help eliminate spatter in GMAW of Mg alloys and that cleaning the filler metal with sandpaper to remove $Mg(OH)_2$ can help eliminate hydrogen porosity (Ref. 18). As mentioned previously, the workpiece surface in the welding area was also

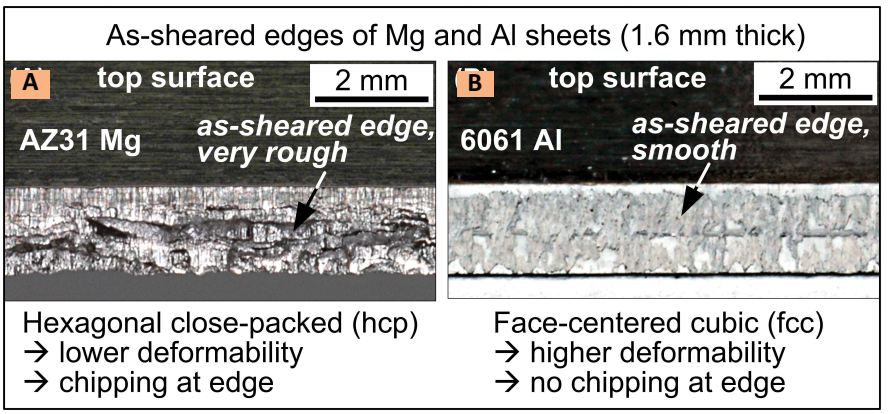

Fig. 6 — As-sheared edges of 1.6-mm-thick sheets. A — Rough edge of AZ31B Mg (~Mg-3Al-1Zn-0.2Mn) showing chipping near bottom of edge; B — smooth edge of 6061 (~Al-1Mg-0.6Si) showing no chipping. Hexagonal close-packed (hcp) structure, with fewer slip planes available, is less deformable than face-centered cubic (fcc) structure.

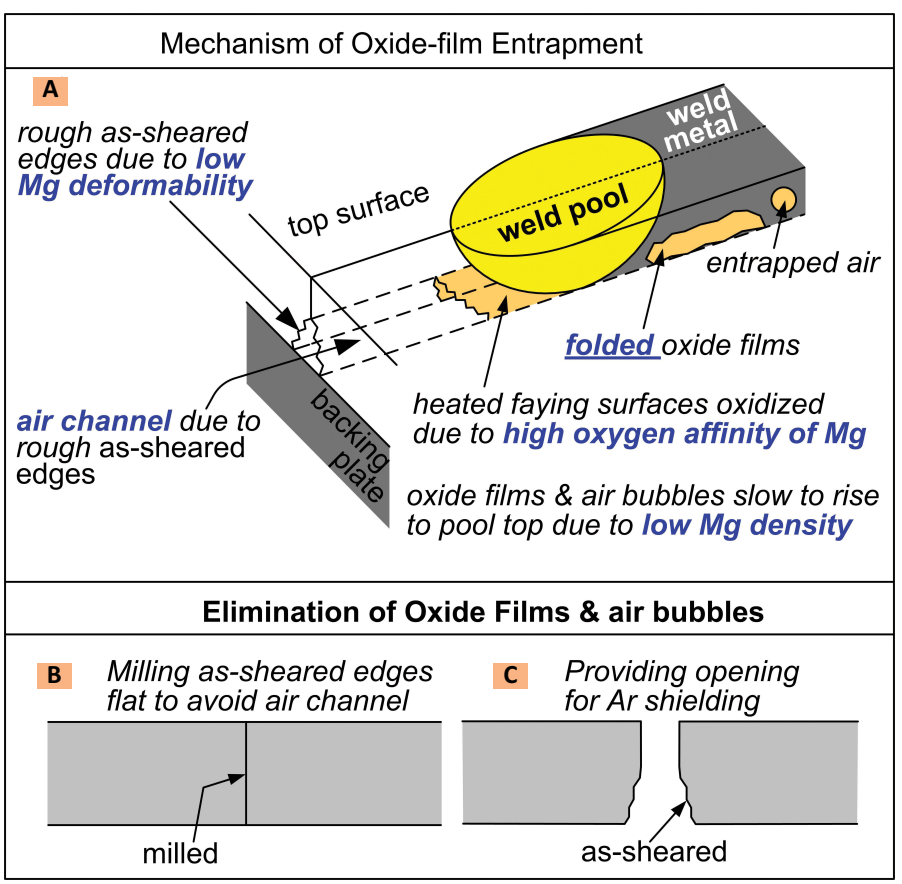

Fig. 7 — Mechanism and elimination of oxide-film entrapment. A — Mechanism; B — elimination by milling edges after shearing; C — elimination by leaving an opening.

cleaned before welding.

Tensile testing results of the specimens prepared from the butt joint welds show that good weld quality can be achieved by CSC-GMAW. Except in the presence of defects such as entrapped oxide films and air in the fusion zone, which will be discussed subsequently, failure occurred outside the fusion zone along the fusion boundary.

Sound welds can be made without entrapments of oxide films and without a high crown. The average joint strength of a sound weld can be close to that of the base metal (290 MPa) as shown in Fig. 4. The compositions of the welds were calculated based on the dilution and the compositions of the workpiece and filler metal. The dilution is defined as the percentage of the melted base metal in the weld metal, that is, the extent the filler metal is diluted by the base metal (Ref. 20).

For weld 007, the dilution is about 44%, and the weld metal composition is thus Mg-4.7Al-1Zn-0.27Mn. As for weld #008, the dilution is 41% and the weld metal composition is thus Mg-4.8Al-1Zn-0.28Mn. The joint ductility, about 8 to 9% elongation before failure, is well below that of the base metal (29%). The tensile tested base-metal specimen showed clear necking (i.e., to less than the initial width of 25.4 mm) near the mid length of the specimen. Obviously, in the weld specimen such necking is hindered by the top and bottom reinforcements of the weld. In fact, the weld and its surrounding area bent and were no longer flat though still straight. In the study by Song et al. (Ref. 21) on butt joint welding of 3-mm-thick AZ31 Mg sheets by AC-pulsed GMAW, a high strength level close to that of the base metal was also reported and the elongation before failure varied from 6 to 9%.

Although sound butt joint welds can be made, precautions need to be taken to avoid two defects that have not been discussed or even noticed or observed previously in GMAW of Mg alloys: 1) entrapped oxide films, and 2) high crowns. As found in the present study, they tend to form very easily and they can degrade the weld quality significantly, especially the ductility. These issues and the methods to deal with them are discussed below.

Issue 1: Entrapment of Oxide Films

It was observed that oxide films can be very easily trapped in the fusion zone. However, entrapment of oxide films and air is mainly caused by the combination of unusual physical properties of Mg rather than the welding process used, as will be explained subsequently.

Figure 5 shows weld 002, which was made with the as-sheared faying surfaces (Fig. 5A) in contact with each other to form a butt joint. The top sur-

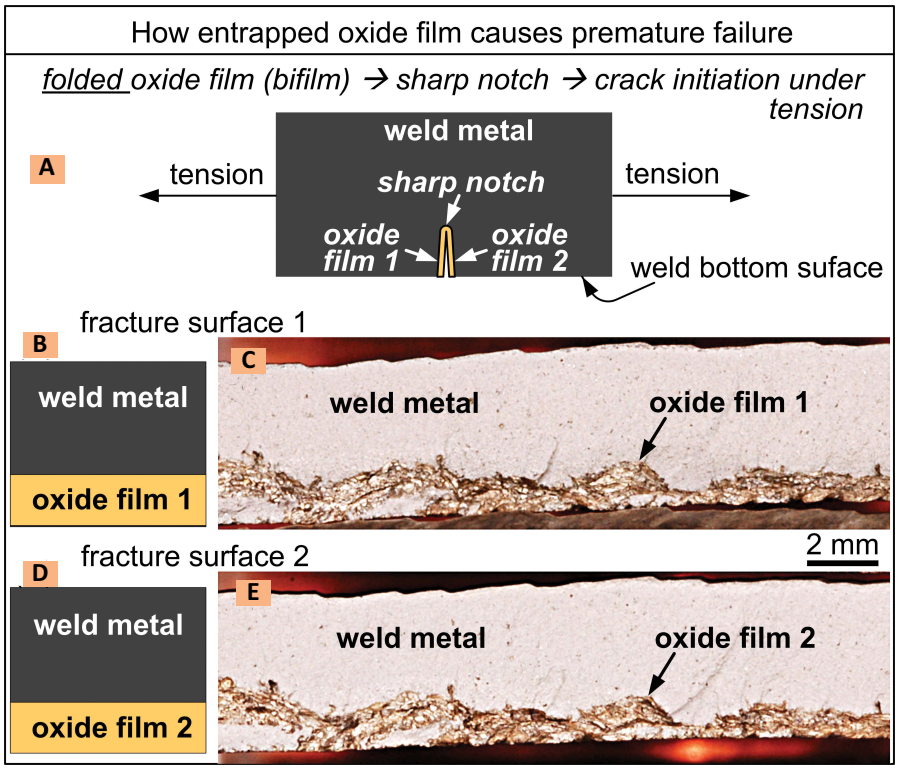

Fig. 8 — Folded oxide film as a potential site of crack initiation. A — Schematic illustration of transverse cross-section of fusion zone; B, D — schematic fracture surfaces; C, E — fracture surfaces of tensile tested specimen (butt joint weld 051) confirming existence of bifilm.

face (Fig. 5B) shows the weld is free of spatter or open holes caused by hydrogen porosity. The transverse cross-section of the weld (Fig. 5C) shows a toe angle of about 135 deg, which is the angle between the crown and workpiece top surface. The tensile test curves (Fig. 5D) show that the ductility (elongation before failure) scatters significantly from specimen to specimen of the same weld, from about 9% in specimen 4 to 7% in specimen 5 and 6% in specimen 2. The tensile test curve of specimen 1 is similar to that of specimen 4 but not included because of accidental slippage at the beginning of tensile testing. It should be pointed out that elongation in a transverse tension specimen does not give an accurate assessment of ductility due to the geometry of the weld itself and the differences in strength of the base metal, weld metal, and heat-affected zone. The elongation at failure shown in Fig. 5D and subsequent figures is not meant to represent the actual weld ductility but just for comparing the levels of ductility of different welds.

The side views of the tensile-tested specimens (Fig. 5E) show the locations of failure. Specimens 2 and 5 failed inside the fusion zone while the rest of the specimens failed outside the fusion zone along the weld, that is, in the partially melted zone (Ref. 20). The fracture surface of specimen 5 (Fig. 5F) shows entrapped oxide films in the fusion zone along the welding direction. The left side of the fracture surface corresponds to the photo of specimen 5 shown in Fig. 5E. As shown, air can be entrapped inside the oxide films. The gas holes are air holes because there was no hydrogen on the faying surfaces during welding to cause hydrogen porosity. The faying surfaces were welded shortly after preparation and cleaned with acetone before welding. Oxide films were also observed on the fracture surface of specimen 2 (not shown). Thus, it is clear from Fig. 5 that oxide films in the

Table 5 — Current Settings for Butt Joint Welding with a Root Opening of 1.0 or 1.2 mm

Weld #	Arc Time						Short Circuit Time					
	Start		Mid		End		Start		Mid		End	
	Current (A)	Time (ms)	Current (A)	Time (ms)	Current (A)	Time (ms)	Current (A)	Time (ms)	Current (A)	Time (ms)	Current (A)	Time (ms)
G001	45	4.0	55	6.0	45	n/a	70	2.0	70	4.0	64	n/a
G002	60	4.0	50	6.0	60	n/a	70	2.0	70	4.0	64	n/a
G003	42	4.0	52	6.0	42	n/a	70	2.0	70	4.0	64	n/a
G004	42	4.0	52	6.0	42	n/a	70	2.0	70	4.0	64	n/a
G005	41	4.0	51	6.0	41	n/a	70	2.0	70	4.0	64	n/a
G006	41	4.0	51	6.0	41	n/a	70	2.0	70	4.0	64	n/a
G007	40	4.0	50	6.0	40	n/a	70	2.0	70	4.0	64	n/a
G008	40	4.0	50	6.0	40	n/a	70	2.0	70	4.0	64	n/a
G009	38	4.0	48	6.0	38	n/a	70	2.0	70	4.0	64	n/a
G010	38	4.0	48	6.0	38	n/a	70	2.0	70	2.5	64	n/a
G011	37	4.0	47	6.0	37	n/a	70	2.0	70	2.5	64	n/a

Rise Rate of Current (A/ms): 250; Fall Rate of Current (A/ms): 250

ms: milliseconds.

fusion zone along the welding direction can significantly decrease the ductility.

Mechanism of Oxide-Film Entrapment

In order to understand how oxide films are entrapped in butt joint welds of Mg alloys, the faying surfaces before welding were examined.

Figure 6 shows the as-sheared edges of an AZ31Mg sheet and a 6061 Al (~Al-1Mg-0.6Si) sheet, both prepared with the same shear. Chipping is evident near the bottom of the AZ31 Mg edge (Fig. 6A), which makes the lower portion of the edge rough. Chipping was observed on all sheared edges, parallel or normal to the rolling direction, and welds were made parallel to the rolling direction. The hexagonal close-packed (hcp) structure of Mg and its alloys does not provide many slip planes for plastic deformation (Ref. 22). Unable to deform much plastically, Mg sheets tend to chip off during shearing. No chipping is visible on the as-sheared 6061 Al edge (Fig. 6B). Unlike Mg, the face-centered cubic (fcc) structure of Al and its alloys provides more slip planes for plastic deformation to occur more easily.

The mechanism of oxide-film entrapment in butt joint welding of as-sheared Mg sheets is proposed in Fig. 7. When two as-sheared rough edges are put together to form a butt joint, an air channel exists between the lower portions of the faying surfaces (Fig.

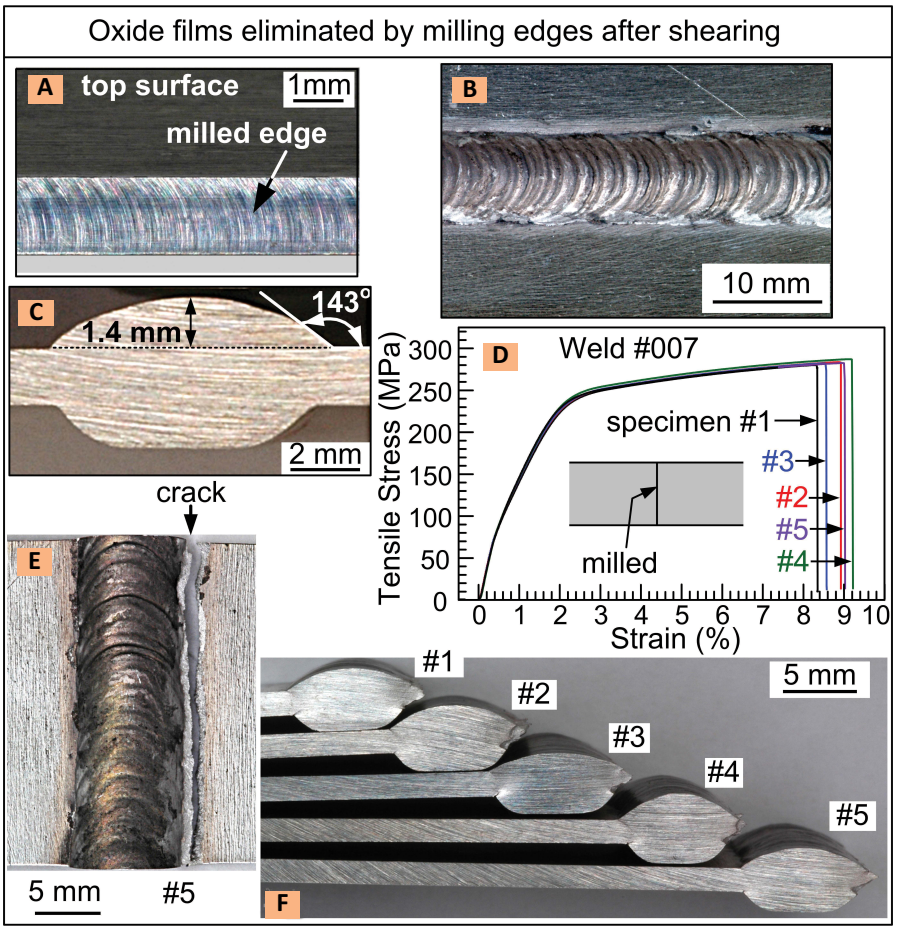

Fig. 9 — Elimination of oxide films from weld 007. A — Milling of edge after shearing; B — top view; C — transverse cross section; D — tensile test curves; E — top view of specimen 5 showing fracture along fusion boundary; F — side views of tensile tested specimens. Unlike weld 002 (Fig. 5), no specimens here show significant ductility reduction caused by oxide films.

Table 6 — Wire-Speed Settings for Butt Joint Welding with a Root Opening of 1.0 or 1.2 mm

	Wire Speed						
	Down		Up 1		Up 2	Arc	Penetration
Weld #	Wire Down Speed (MPM)	Delay before Wire Down (ms)	Wire Up 1 Speed (MPM)	Delay before Wire Up (ms)	Wire Up 2 Speed (MPM)	Length (mm)	Delay (ms)
G001	15	0	15	0	15	0.2	0
G002	15	0	15	0	15	0.2	0
G003	6.8	4	6.8	6	6.8	0.2	0
G004	6.8	4	6.8	6	6.8	0.2	0
G005	6.8	4	6.8	6	6.8	0.2	0
G006	6.8	4	6.8	6	6.8	0.2	0
G007	6.8	4	6.8	6	6.8	0.2	0
G008	6.8	4	6.8	6	6.8	0.2	0
G009	6.8	4	6.8	6	6.8	0.2	0
G010	6.8	4	6.8	6	6.8	0.2	0
G011	6.8	4	6.8	6	6.8	0.2	0

MPM: meters per minute, ms: milliseconds.

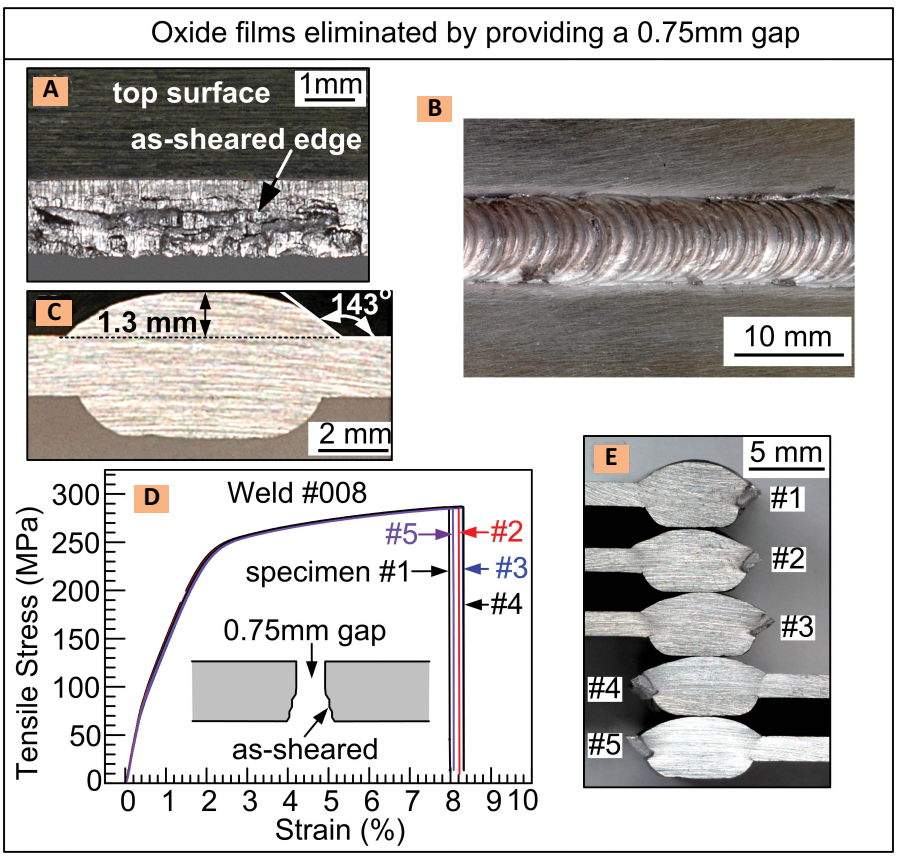

Fig. 10 — Elimination of oxide films from weld 008. A — Rough edge caused by shearing; B — top view of weld; C — transverse cross section; D — tensile-testing curves; E — side views of tensile tested specimens. Unlike weld 002 (Fig. 5), no specimens here show significant ductility reduction caused by oxide films.

7A). The channel is inaccessible by the Ar shielding gas from the torch above the workpiece. During welding the faying surfaces ahead of the weld pool are heated up. The tendency for metals to oxidize is shown by the Ellingham diagram for oxides (Ref. 23), which is a plot of the free energy of oxide formation vs. temperature. The Ellingham diagram shows that Mg is one of the metals with the strongest tendency to oxidize, stronger than Al (Ref. 23). The combination of air, heating, and the very high oxidation tendency of Mg causes oxide films to form on the faying surfaces ahead of the weld pool. Because of the very low density of Mg, the oxide films and air bubbles entrapped in the weld pool may not be able to rise quickly and escape from the weld pool. The air channel can be avoided as shown in Fig. 7B and C, which are discussed subsequently.

Figure 8 explains how an entrapped oxide film can cause premature failure of a weld. A folded oxide film present along the central plane of the fusion zone can provide a very sharp notch to initiate crack under tension — Fig. 8A. The resultant two fracture surfaces should each show the presence of an oxide film — Fig. 8B, D. This is confirmed by the actual fracture surfaces of the tensile-tested

Table 7 — Summary of Butt Joint Welds Made with a Root Opening < 1 mm

Weld #	Butt Joint	Power (W)	Travel Speed (in./min)	Weld Penetration	UTS (MPa)	Elongation (%)	% Base Metal UTS
002	1.18-mm groove; no root opening	922	18	full	275.7	7.3	94.8
007	1.18-mm groove milled flat; no root opening	885	18	full	283.2	8.8	97.6
008	1.18-mm groove; 0.75-mm root opening	903	18	full	285.8	8.2	98.4
047	0.77-mm groove; 0.5-mm root opening	932	34	full	273.5	6.5	94.2
049	0.77-mm groove; 0.5-mm root opening	902	26	full	269.7	5.2	92.9
051	0.77-mm groove; 0.5-mm root opening	895	18	full	261.9	4.6	90.2
052	0.77-mm groove milled flat; no root opening	841	18	full	263.5	4.1	90.8
053	0.77-mm groove milled flat; no root opening	874	26	full	260.1	4.1	89.6
054	square groove milled flat; no root opening	877	34	full	246.5	3.1	84.9
056	1.18-mm groove; no root opening	971	18	full	–	–	–
	AZ31B base metal				290.3	29.4	100.0

specimen of a butt joint weld (Fig. 8C, E), that is, specimen 3 of weld 051 (to be shown discussed subsequently). Note that the oxide films on the two fracture surfaces are nearly exact mirror images of each other.

Campbell (Ref. 24) reported that oxide films can significantly degrade metal castings. He showed how oxides films can be introduced into the bulk liquid metal just by pouring the liquid metal into a crucible. For instance, the oxide films covering the surface of the liquid metal already in the crucible can be pushed into the bulk liquid metal by the stream of liquid metal still being poured into the crucible. When an oxide film is folded, it can provide a very sharp notch to significantly degrade the resultant casting. Campbell (Ref. 24) called this double film defect a "bifilm" as a convenient short-hand to emphasize its double nature. The faying surfaces in butt joint welding might be a potential source for bifilms to form along the weld central plane and degrade the resultant weld. The fact that the oxide films on the two fracture surfaces of the tensile tested specimen (Fig. 8C, E) are nearly exact mirror images of each other suggests the presence of bifilms. It is interesting to note that Coniglio and Cross (Ref. 25) discussed the possible role of bifilms in the initiation of cracks during weld-metal solidification.

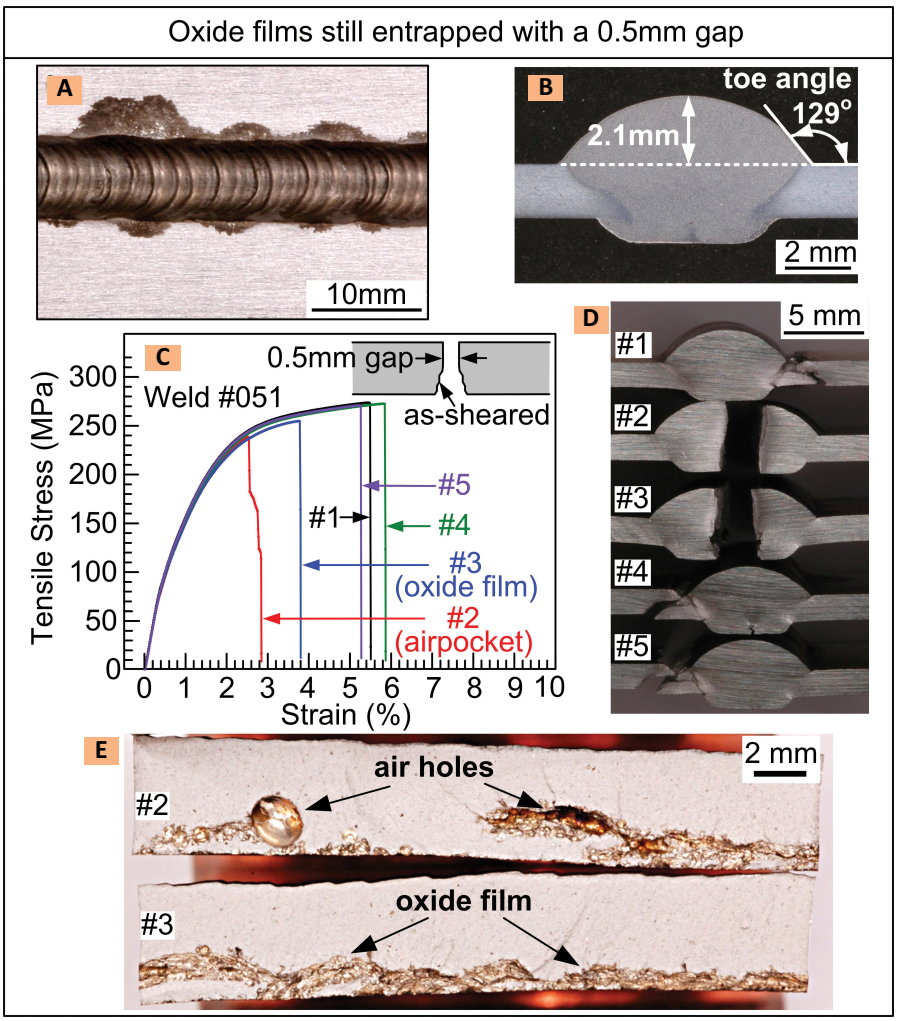

Fig. 11 — Entrapment of oxide films in weld 051 caused by too small an opening between as-sheared faying surfaces. A — Top view; B — transverse cross section; C — tensile test curves showing lower ductility of specimens 2 and 3; D — failure through fusion zones of specimens 2 and 3; E — fracture surfaces of specimens 2 and 3 (not 1, 4, and 5) showing entrapped oxides and air.

Reducing Entrapment by Milling Faying Surfaces

One way to reduce entrapment of oxide films in the fusion zone is to mill the rough as-sheared faying surfaces smooth before welding. This can eliminate the air channel that causes the entrapment. Figure 9 shows a butt joint weld, weld 007, made with the faying surfaces milled flat after shearing — Fig. 9A. As compared to weld 002 made with as-sheared faying surfaces (Fig. 5), the tensile test curves (Fig. 9D) show significantly less scatter in ductility. The tensile-tested specimens (Fig. 9E, F) show failure along the outside of the fu-

Table 8 — Summary of Butt Joint Welds Made with a Root Opening of 1.0 or 1.2 mm

Weld #	Butt Joint	Power (W)	Travel Speed (in./min)	Weld Penetration
G001	1.18-mm square groove; 1.0-mm root opening	639	18	Partial
G002	1.18-mm square groove; 1.0-mm root opening	857	18	Melt-through
G003	1.18-mm square groove; 1.2-mm root opening	742	18	Melt-through
G004	1.18-mm square groove; 1.2-mm root opening	727	18	Full
G005	1.18-mm square groove; 1.2-mm root opening	735	18	Full
G006	1.18-mm square groove; 1.2-mm root opening	764	18	Melt-through
G007	1.18-mm square groove; 1.2-mm root opening	738	18	Full
G008	1.18-mm square groove; 1.2-mm root opening	768	18	Melt-through
G009	0.44-mm square groove; 1.2-mm root opening	636	18	Full
G010	0.65-mm square groove; 1.2-mm root opening	650	18	Full
G011	0.65-mm square groove; 1.2-mm root opening	628	18	Full

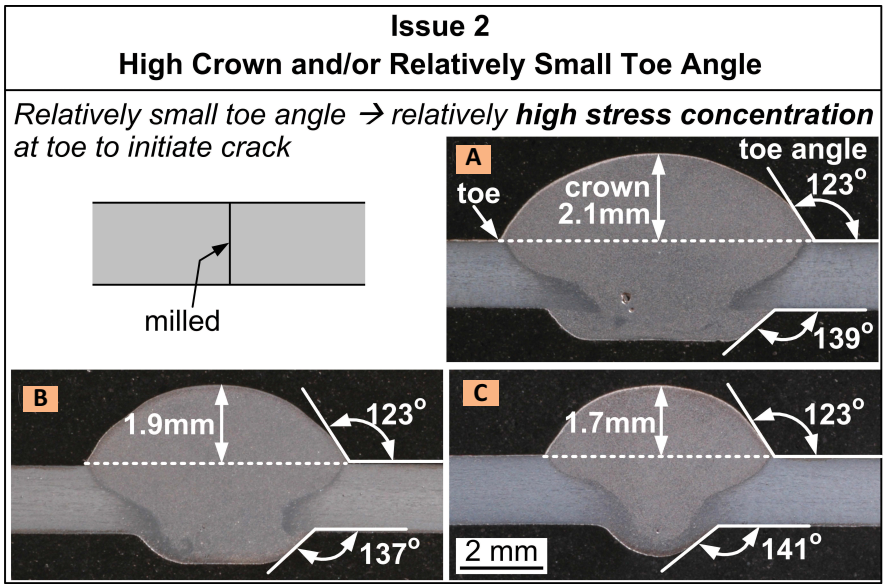

Fig. 12 — High crowns on butt joint welds made at travel speeds of the following: A — 7.6 mm/s (18 in./min, weld 052); B — 11.0 mm/s (26 in./min, weld 053); C — 14.4 mm/s (34 in./min, weld 054). Crown height is reduced by increasing travel speed but the toe angle remains relatively small at 123 deg.

sion zone, consistent with the absence of oxide-film entrapment. No air holes are visible in the fusion zone — Fig. 9F.

Reducing Entrapment by Separating Faying Surfaces

Another way to help avoid entrapment of oxide films in the fusion zone is to leave an opening between as-sheared faying surfaces. Since Ar is heavier than air (Ref. 20), the Ar shielding gas from the torch may enter the opening near the weld pool and keep air away. If oxide films still form on the surfaces, the liquid filler metal may be able to carry them away while going through the opening.

Figure 10 shows a weld, weld 008, made with a 0.75-mm opening between two as-sheared faying surfaces — Fig. 10A. The tensile test curves (Fig. 10D) show significantly less scatter in ductility. Failure occurs along the outside of the fusion boundary (Fig. 10E), consistent with the absence of entrapped oxide films in the fusion zone. The effectiveness of a root opening in eliminating entrapment of oxide films can be affected by the width of the opening. A smaller opening allows less room for Ar to purge the air between the surfaces and for the liquid filler metal to flow through and carry oxide films away from the surfaces (if oxide films are present).

Figure 11 shows a butt joint weld (weld 051) made with a 0.5-mm opening between two as-sheared faying surfaces in the as-sheared condition. The tensile test curves (Fig. 11C) show much scatter in the ductility, with specimens 2 and 3 being the lowest. Tensile tested specimens 2 and 3 (Fig. 11D) show failure through the fusion zone and oxide films and air bubble on the fracture surfaces — Fig. 11E. Besides less room for both Ar purging and filler-metal flow, weld 051 is considerably narrower than weld 008 — Fig. 10. The larger weld pool in the case of weld 008 can be expected to provide more room for strong fluid flow to exist (Ref. 26) and carry the entrapped oxide films away from the faying surfaces.

Still another way to help reduce entrapment of oxide films is to provide additional Ar shielding gas from below. For instance, a backing plate can be designed to allow Ar purging from under the butt joint.

It is worth noting that, referring to Fig. 7C, flipping over the as-sheared sheets without providing an opening in between may not always work. It is true that flipping over the as-sheared sheets resembles a butt joint design with a single-V groove to allow the Ar shielding gas to reach the heated faying surfaces immediately ahead of the weld pool and thus protect it from oxidation. However, close examinations of as-sheared edges have revealed that chipping some-

Table 9 — Current Settings for Lap Welding

Weld No.	Current											
	Arc Time						Short Circuit Time					
	Start		Mid		End		Start		Mid		End	
	Current (A)	Time (ms)	Current (A)	Time (ms)	Current (A)	Time (ms)	Current (A)	Time (ms)	Current (A)	Time (ms)	Current (A)	Time (ms)
012	67	4.0	88	10.0	78	n/a	96	2.5	106	3.0	85	n/a
016	59	4.0	80	10.0	70	n/a	96	2.5	106	3.0	85	n/a
018	55	4.0	76	10.0	66	n/a	96	2.5	106	3.0	85	n/a
019	55	4.0	76	10.0	66	n/a	96	2.5	106	3.0	85	n/a
020	55	4.0	76	10.0	66	n/a	96	2.5	106	3.0	85	n/a
022	74	4.0	95	10.0	85	n/a	96	2.5	106	3.0	85	n/a
025	53	4.0	74	10.0	64	n/a	96	2.5	106	3.0	85	n/a
031	70	5.0	90	15.0	80	n/a	110	2.5	130	4.0	105	n/a

Rise rate of current (A/ms): 250; fall rate of current (A/ms): 250

ms: milliseconds.

times occurs at the mid height of a sheared edge. That is, the rough portion of an as-sheared edge can be at its mid height instead of at its bottom. Thus, air pockets can still exist between the two faying surfaces to cause oxidation and air bubbles if the as-sheared sheets are just flipped over to form a butt joint without an opening.

Issue 2: High Weld Crowns

It was found that a high weld crown tends to form on a butt joint weld very easily and that a higher crown tends to be associated with lower ductility in tensile testing. As is discussed subsequently, the low fluidity of liquid Mg is responsible for the high crowns of butt joint welds, but made worse by the lower heat input in short-circuiting type GMAW. As mentioned previously, Lockwood (Ref. 10) and Rethmeier et al. (Ref. 12) both showed high crowns on butt joint welds made with short-circuiting type GMAW though no explanations were given.

Figure 12 shows the crown height can be significantly greater than the workpiece thickness (1.6 mm). These welds were made with faying surfaces milled flat after shearing and without an opening, welds 052 (Fig. 12A) at 7.6 mm/s, weld 053 (Fig. 12B) at 11.0 mm/s, and weld 054 (Fig. 12C) at 14.4 mm/s. As shown, increasing the travel speed tends to decrease the crown height. However, the toe angle remains unchanged at about 123 deg. This, perhaps, is not surprising because the time available for the liquid pool to spread out also decreases as the travel speed increases.

For the purpose of discussion, a toe angle significantly less than 135 deg (weld 002 in Fig. 5C), for instance 130–110 deg, will be called a relatively small toe angle. A relatively small toe angle means a more abrupt thickness change and hence a significantly higher stress concentration at the toe. A high stress concentration tends to act as a crack initiation site under tension or cyclic tensile loading and leads to premature failure. A relatively small toe angle can significantly reduce the fatigue resistance of the weld (Ref. 20). As is shown subsequently, a relatively small toe angle tends to be associated with a lower ductility in tensile testing.

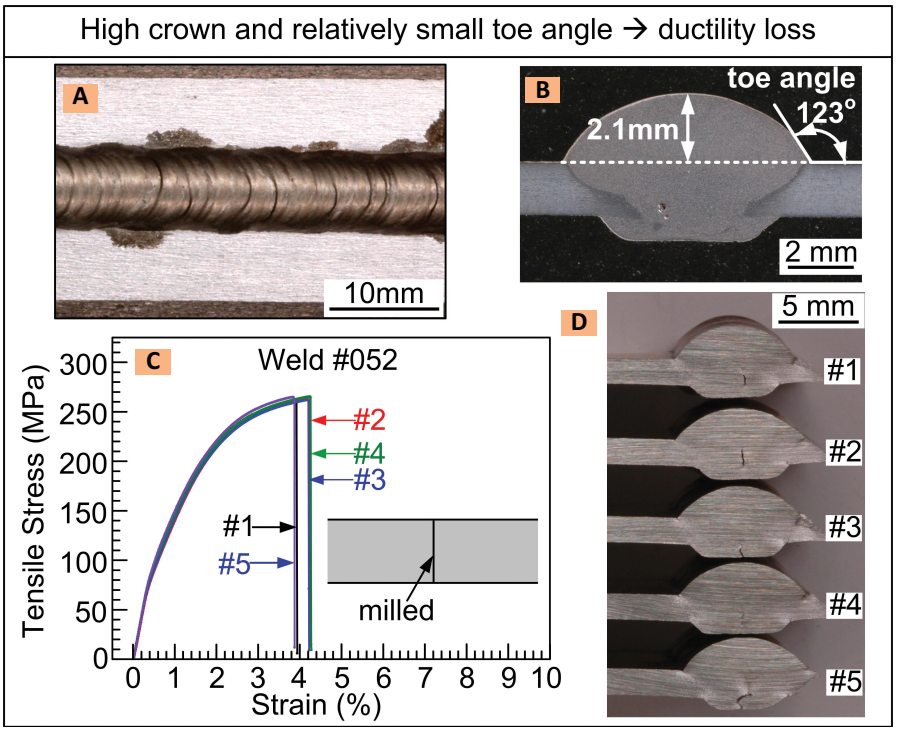

Fig. 13 — Weld 052 with a high crown. A — Top view of weld; B — transverse cross section; C — tensile test curves; D — side views of tensile-tested specimens. Crown is higher, toe angle smaller, and ductility lower than weld 007 — Fig. 9.

Table 10 — Wire-Speed Settings for Lap Welding

	Wire Speed						
	Down		Up 1		Up 2		
Weld No.	Wire Down Speed (MPM)	Delay before Wire Down (ms)	Wire Up 1 Speed (MPM)	Delay before Wire Up (ms)	Wire Up 2 Speed (MPM)	Arc Length (mm)	Penetration Delay (ms)
012	13.0	2	13.0	3	13.0	0.3	0.8
016	25.0	4	25.0	6	25.0	0.2	0.8
018	19.0	4	19.0	6	19.0	0.2	0.0
019	19.0	4	19.0	6	19.0	0.2	0.0
020	19.0	4	19.0	6	19.0	0.2	0.0
022	14.8	4	14.8	6	14.8	0.2	0.8
025	13.0	2	13.0	3	13.0	0.2	0.4
031	25.0	0	25.0	0	25.0	0.2	0

MPM: meters per min, ms: milliseconds.

Weld 052 made at the lowest travel speed of 7.6 mm/s is shown further in Fig. 13. The transverse cross-section macrograph — Fig. 13B shows a high crown of 2.1 mm. Tensile testing (Fig. 13C) indicates a low ductility of about 4%, about one half of the 8–9% of welds 007 (Fig. 9) and 008 — Fig. 10. The tensile tested specimens show failure outside the fusion zone — Fig. 13D. In view of the absence of entrapped oxide films on their fracture surfaces, the low ductility is likely to be caused by the relatively small toe angle. Since welds 052, 007, and 008 were made under similar welding parameters, the extent of recrystallization and grain growth in the heat-affected zone (HAZ) can be expected to be similar in these welds. Thus, the lower ductility of weld 052 cannot be caused by the differences in the HAZ. Weld 053 made at the intermediate travel speed of 11.0 mm/s showed

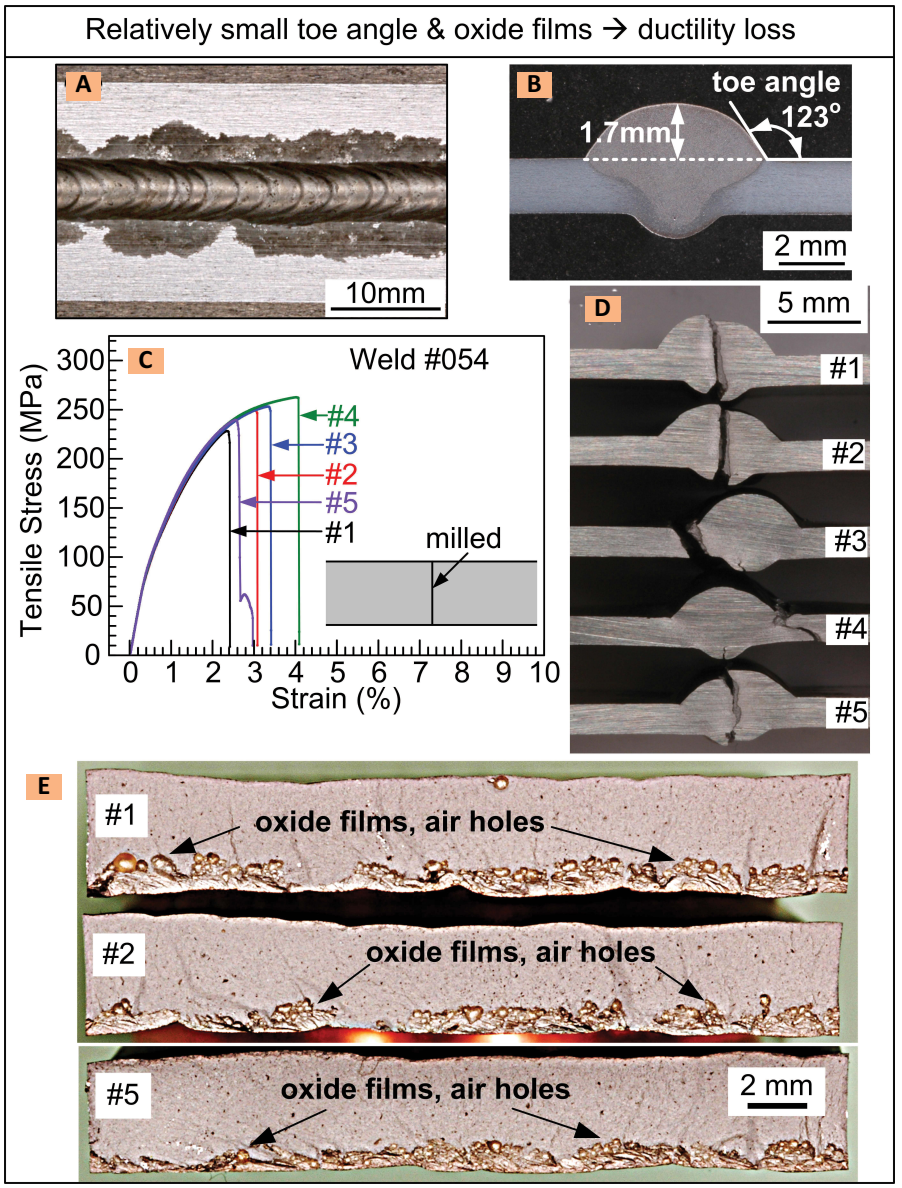

Fig. 14 — Weld 054 with a high crown. A — Top view; B — transverse cross section; C — tensile test curves; D — side views of tensile-tested specimens; E — fracture surfaces of specimens 1, 2, and 5 (not 3 and 4) showing entrapment of oxide films and air in spite of milling faying surfaces after shearing.

similar results as weld 052.

Weld 054 made at the highest travel speed of 14.4 mm/s is shown further in Fig. 14. The transverse cross section (Fig. 14B) shows that the crown height is now reduced to 1.7 mm but the toe angle is still relatively small at 123 deg. The tensile test curves (Fig. 14C) show a highest ductility value of only about 4% in specimen 4, and even lower values of about 2–3% in specimens 1, 2, and 5. Tensile-tested specimens (Fig. 14D) show failure through the fusion zone and fracture surfaces (Fig. 14E) show entrapped oxide films and air in specimens 1, 2, and 5. The entrapment is surprising because the faying surfaces were milled flat after shearing and put together without an opening. It is likely that a very small space and hence some residual air still existed between the faying surfaces, enough to cause oxidation in view of the very high affinity of Mg for oxygen. Perhaps with a significantly larger weld pool such as that associated with the bigger weld (weld 007 in Fig. 9), fluid flow may be stronger to carry the oxide films away from the faying surfaces.

Mechanism of High-Crown Formation

The cause of high crowns is discussed as follows. Since no high crowns were encountered during similar butt joint welding of Al sheets by CSC-GMAW, the physical properties of Mg are compared against those of Al when considering the following three factors.

The first factor is the γ/ρ ratio, where γ and ρ are the surface tension and density of the liquid metal, respectively. It is well known in floating-zone crystal growth that the maximum height of the molten zone in a vertical solid rod that can be supported by its own surface tension is proportional to the square root of the γ/ρ ratio (Ref. 27). Thus, the crown height may also increase with increasing γ/ρ. In fact, Campbell (Ref. 24) derived an equation to show that the height of a sessile drop on a substrate is proportional to the square root of the γ/ρ ratio. The physical properties of the weld pool depend on the weld pool composition, which in turn depends on the workpiece composition, filler-metal composition, and dilution level (Ref. 20). Since the physical properties of the weld pool are not available, those of pure Mg and Al are used in the discussion as an approximation. For Mg, γ = 5590 dyne/m, ρ = 1700 kg/m^3 and thus γ/ρ = 3.29 dyne m^2/kg. As for Al, γ = 9140 dyne/m, ρ = 2700 kg/m^3 and thus γ/ρ = 3.39 dyne m^2/kg (Ref. 28). Since the γ/ρ ratio is nearly identical for both Mg and Al, the tendency for Mg to have high crowns is unlikely to be caused by a much higher γ/ρ ratio.

The second factor to be considered is the conduction of heat away from the liquid metal to cause solidification. The thermal conductivity k is 153 W/(m K) for Mg and 237 W/(m K) for Al (Ref. 29). Thus, the lower thermal conductivity of Mg suggests that the high Mg weld crown is not caused by the faster heat extraction from and hence solidification of liquid Mg. The thermal diffusivity α equals to $k/(\rho/C_p)$, where C_p is the heat of fusion. C_p is 1.05 J/(g K) for Mg and 0.91 J/(g K) for Al (Ref. 30). Thus, α is 86 mm^2/s for Mg and 97 mm^2/s for Al. Thus, the lower thermal diffusivity of

Mg also suggests that the high crown is not caused by the faster heat extraction from and hence solidification of liquid Mg.

The third factor to be considered is the low volumetric heat content of liquid Mg. The very low density of Mg reduces the amount of heat needed to be removed per unit volume of liquid Mg to be solidified. For comparison, the heat of fusion and specific heat of Al are, respectively, 398 J/g and 0.91 J/(g K). Multiplying them by the density of Al (2700 kg/m^3) yields a 1.075×10^9 J/m^3 volumetric heat of fusion and a 2.46×10^6 J/(m^3 K) volumetric specific heat of Al. As for Mg, the heat of fusion and specific heat are, respectively, 368 J/g and 1.05 J/(g K), which are close to those of Al. However, the density of Mg, 1700 kg/m^3, is about one-third lower than that of Al, 2700 kg/m^3 (Ref. 30). Upon multiplication by the density of Mg, the volumetric heat of fusion of Mg becomes 6.26×10^8 J/m^3 and the volumetric specific heat 1.79×10^6 J/(m^3 K), which are significantly lower than those of Al. Thus, because of the significantly lower density of Mg, the sensible heat needed to be removed to cool down the same liquid volume is 27% less for Mg than for Al, and the latent heat needed to be removed to solidify the same liquid volume is 42% less for Mg than for Al. In fact, this is exactly why Mg die castings can be made significantly faster than Al ones (Ref. 31). In Mg casting, the steel mold extracts heat from the liquid metal. In Mg welding, the steel backing plate and the base metal extract heat from the liquid metal.

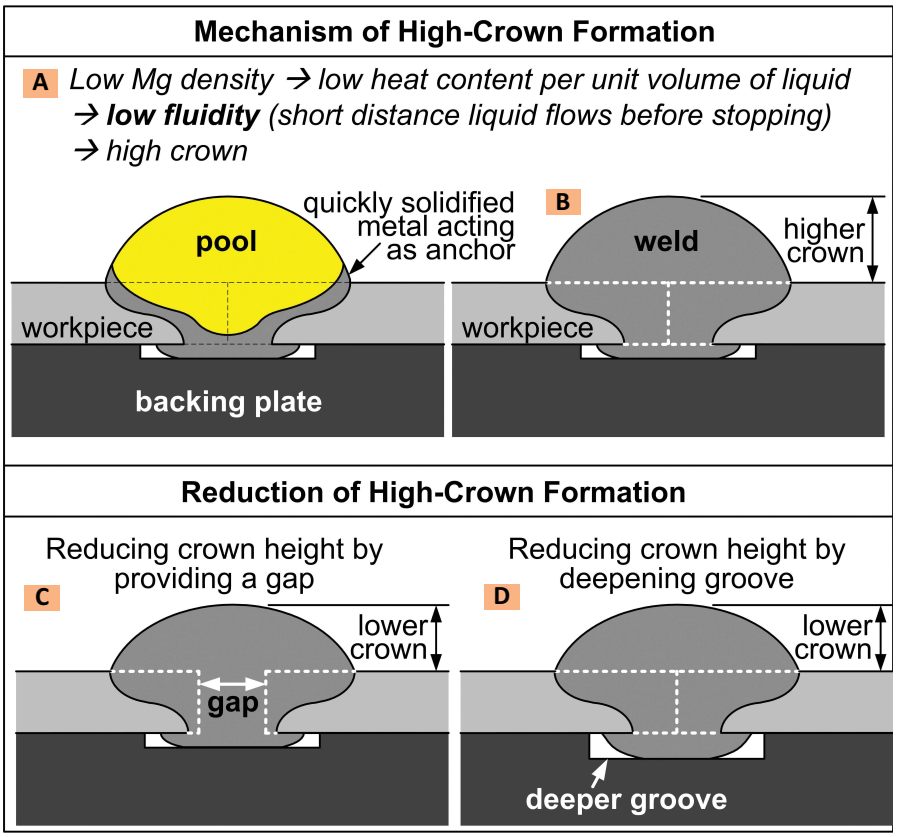

Fig. 15 — Mechanism and reduction of high-crown formation. A — Mechanism; B — high weld crown; C — crown-height reduction by providing an opening to help both accommodate filler metal deposit and let liquid metal quickly penetrate the workpiece; D — crown height reduction by deepening the groove in the backing plate to help accommodate filler metal deposit.

It should be mentioned that in metal casting, the distance the liquid metal can flow before stopping is called the fluidity. The fluidity is proportional to the volumetric heat content (both the latent heat and the superheat) of the liquid and the diameter of the channel in the mold through which the liquid metal flows (Ref. 31). It is inversely proportional to the heat transfer coefficient between the liquid metal and mold, and the difference between the melting point and mold temperature. The melting point of Mg (650°C) is close to that of Al (660°C). The heat transfer coefficient between

Table 11 — Summary of Lap Welds

Weld No.	Penetration into Lower Sheet	Average Power (W)	Travel Speed (in./min)	Wire Position from Edge (mm)*	Maximum Tensile Load (N)	Elongation (%)	Maximum Tensile Load (% of Base Metal)
012	full	1335	18	0	6470	1.6	53.2
016	full	1104	18	–0.8	5922	1.4	48.7
018	partial	1033	18	–0.8	6807	1.9	55.9
019	partial/full	1036	18	+0.8	7059	2.0	58.0
020	partial	1031	18	–0.8	7428	2.7	61.0
022	partial/full	1472	18	–5.0	8124	2.7	66.7
025	partial	999	18	+3.1	6775	2.2	55.7
031	partial	1523	24	–0.8	8134	3.2	66.8

* Above upper sheet: < 0; above lower sheet: > 0.

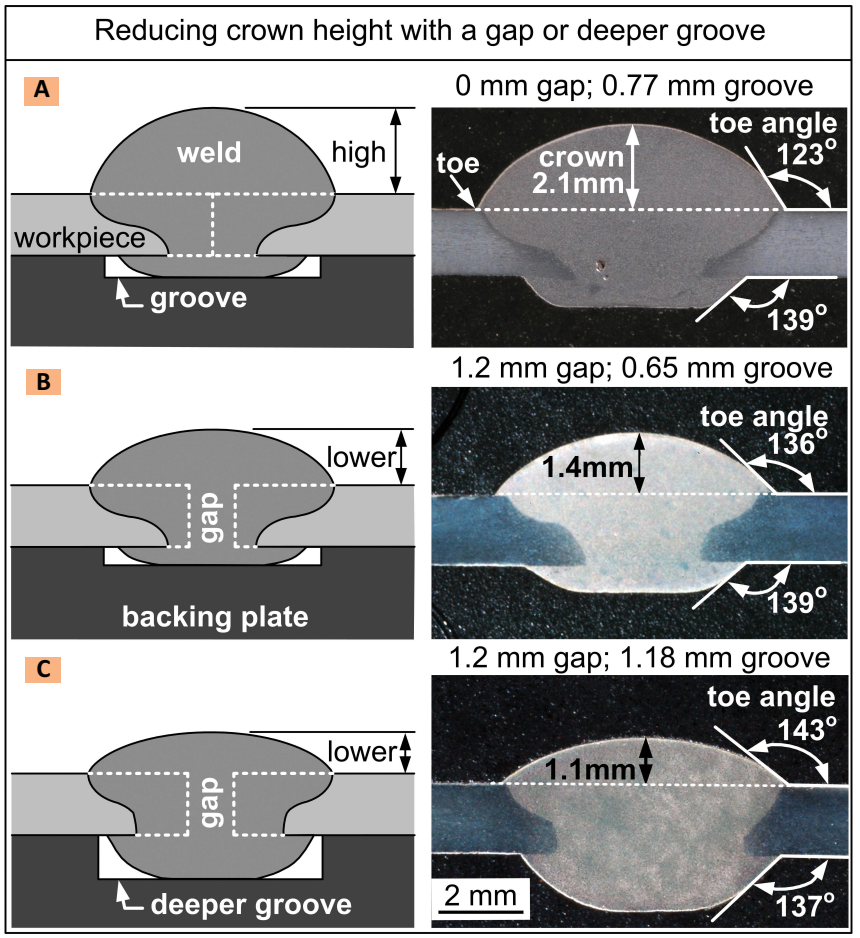

Fig. 16 — High crown in Mg butt joint welding and its reduction. A — High crown caused by low fluidity of liquid Mg; B — crown height reduced with a joint opening; C — crown height further reduced with a deeper groove. The best result may be between B and C.

liquid Mg and solid Mg is likely similar to that between liquid Al and solid Al. Thus, the fluidity of the weld pool in butt joint welding is likely to be proportional to volumetric heat content of liquid.

Therefore, the mechanism of high-crown formation in Mg butt joint welding is as follows: The fluidity of the Mg weld pool is low because of the low density and hence low volumetric heat content. The edge of the weld pool can solidify quickly and act as an anchor to stop its further spreading and hence lowering of the pool height, as illustrated in Fig. 15A and B. In GMAW, the power input is significantly reduced by short circuiting, including CSC-GMAW, in view of the absence of the arc during the short circuit period. Thus, in short-circuiting GMAW superheating of the liquid metal is limited, and this can further reduce the fluidity and promote high crowns.

Figure 15C and D shows the crown height can be reduced by providing a root opening or deepening the groove in the backing plate, respectively. Reducing the wire feed rate may also reduce the crown height. However, since the welding current and hence heat input are also reduced, the volumetric heat content and hence the fluidity can also decrease.

Reducing Crown

Figure 16 is an example showing how the high crown in a Mg butt joint weld (Fig. 16A) can be reduced by widening a joint opening and/or deepening the groove in the backing plate. Widening the opening between the faying surfaces in butt joint welding (Fig. 16B) may help reduce the crown height by accommodating the filler-metal deposit. It may also allow the liquid metal to quickly pass through the opening before solidifying into a high crown. In general, less welding current (slower overall wire feeding) is needed when an opening is provided because there is no need to penetrate the workpiece. Deepening the groove in the steel backing plate provides extra room under the joint to accommodate the filler-metal deposit and reduce the crown height. A deep groove plus a joint opening can make the crown very short (Fig. 16C). Naturally, an excessively large root enforcement caused by too deep a groove is also undesirable.

It was noticed that with a uniform opening of 1.2 mm set up before welding, the opening at the weld-pool front gradually closed as the pool approached the finishing end of the weld. Metals tend to shrink upon solidification because the density of solid metal ρ_S is greater than the density of liquid metal ρ_L. The solidification shrinkage, defined as the ratio of $(\rho_S - \rho_L)/\rho_S$, is 4.2% for Mg (Ref. 31). The problem is that when the root opening gradually shrank because of solidification shrinkage, the pool penetration also gradually decreased. To overcome this problem, the opening was widened linearly from 1.2 mm at the starting end of the weld to 2.0 mm at the finishing end. This was done by putting a short vertical steel wire of 1.2 mm diameter right before the starting end and a similar wire of 2.0 mm diameter right after the finishing end. Driven by shrinkage, the Mg sheets gradually deformed around the wire during welding and reduced the opening to 1.2 mm by the time the weld pool reached the finishing end. In other words, by providing a nonuniform opening that increased from 1.2 to 2.0 mm before welding, a constant weld opening 1.2 mm was obtained after welding. Precautions, however, need to be taken to avoid melt-through during welding when butt joint welding with a wide opening, especially when the groove in the backing plate is deep.

Lap Joint Welding

Tables 9 and 10 show the current settings and the wire-speed settings for lap joint welding, respectively.

Table 11 summarizes the welding conditions and tensile testing results of the resultant lap joint welds.

Issue 3: Formation of Fingers

It was observed that lap joint welds

almost always tended to stick out to the lower sheets as protrusions, which are called "fingers" here. Fingers are caused mainly by the low density of Mg instead of the welding process used as is explained subsequently.

Figure 17 shows lap weld 018. The torch was vertical and moving along the joint line. This direction, in the case of Fig. 17A, is the direction out of the paper. The top view of the weld (Fig. 17B) shows fingers extending from the weld onto the lower sheet. Most fingers do not fuse to the lower sheet well enough to contribute to bonding because their large surface-area-to-volume ratio promotes quick freezing and oxidation. Thus, they tend to decrease the joint strength and cause it to vary along the weld. The transverse cross section of the weld (Fig. 17C) shows a very small toe angle of 55 deg on the lower sheet side of the lap weld. Tensile testing results (Fig. 17D) show ductility (around 2%) significantly lower in lap welds than in butt joint welds (up to about 8%). A lower ductility in lap welds than butt joint welds is expected because lap welds have an intrinsic sharp notch at the fusion boundary between the upper and lower sheets. The tensile tested specimens (Fig. 17E) show failure from the sharp notch through the fusion zone. Specimens 3 and 4 show no bonding between fingers and the lower sheet. The fracture surface shows essentially no oxide films or air bubbles.

It is worth mentioning that fingers were also encountered in the study by Song et al. (Ref. 21). The photograph of the lap joint weld showed clear fingers though they were not mentioned or discussed.

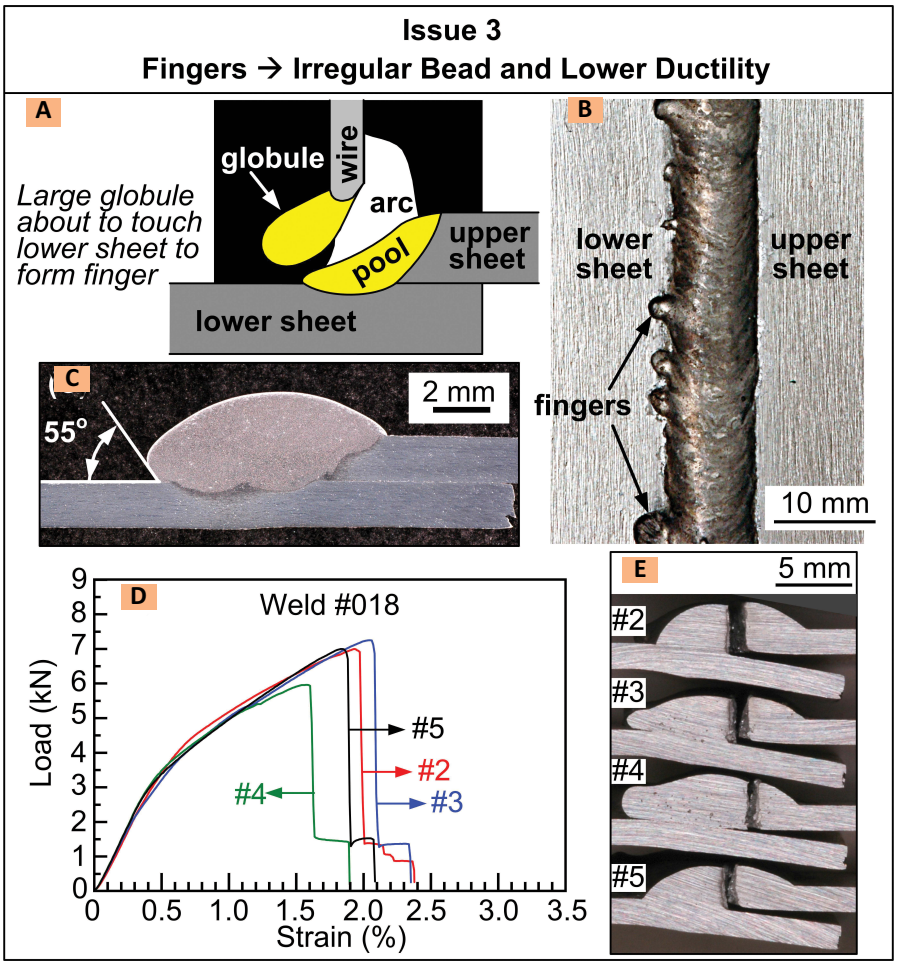

Fig. 17 — Finger formation in lap joint weld 018. A — Schematic sketch of lap joint welding (in the direction out of the paper); B — top view of weld showing "fingers" extending onto lower sheet; C — transverse cross section showing very sharp angle between weld and lower sheet; D — tensile test curves; E — side views of tensile-tested specimens showing failure through fusion zone (from sharp notch between two sheets) and no bonding between fingers and lower sheet (specimens 3 and 4).

Mechanism of Finger Formation

The mechanism is illustrated in Fig. 18A. The very low density of Mg makes the filler metal globule light. Thus, it is difficult for gravity to detach the globule but easy for the arc jet to push it away from the inclined pool surface, as observed by high-speed video (4000 frames/s) (Ref. 18).

Consequently, the globule keeps growing and getting closer to the lower sheet and eventually touches it and quickly solidifies on it as a finger. When the globule touches the lower sheet, it is detached from the welding wire tip and connected to the weld pool. This is why the finger extends from the weld onto the lower sheet. Unlike in conventional GMAW, the welding current is under tight control in CSC-GMAW. Thus, there is no sudden current surge upon short circuiting to cause a sudden arc expansion to expel the globule as spatter.

Eliminating Fingers by Blocking Globule

Figure 18B and C show how to reduce fingers by blocking the filler-metal globule. The blocker can be an inert material such as a steel bar coated with boron nitride (BN) and placed on the lower sheet at a proper distance from the joint line — Fig. 18B. It is intended to keep the growing globule from stretching too far out over the lower sheet to solidify as a finger. The inert blocker can also be mounted on the welding gun to travel with it during welding — Fig. 18C. Fingers can also be eliminated by tilting the welding gun toward the upper sheet (Fig. 18D) as is described subsequently.

Figure 19 shows a lap joint weld (weld 020) made with a stationary blocker — Fig. 19A. The top view (Fig. 19B) shows that the weld edge on the lower sheet is smooth and without any fingers. The transverse cross section (Fig. 19C) shows a 115 deg toe angle, much larger than the 55 deg angle of weld 018 — Fig. 17C. Tensile test results (Fig. 19D) show slightly better

ductility than weld 018 (Fig. 17D) though still low as expected for a lap weld. The tensile tested specimens (Fig. 19E) show failure outside instead of through the fusion zone as in the case of weld 018 — Fig. 17E.

Eliminating Fingers by Tilting Welding Gun

Figure 20 shows a lap joint weld, weld 031, made with the welding gun tilted to shift the globule toward the upper sheet — Fig. 20A. The top view (Fig. 20B) shows that the weld edge on the lower sheet is smooth and without any fingers. The transverse cross section (Fig. 20C) shows a toe angle of 111 deg on the lower sheet. Tensile test results (Fig. 20D) show even better ductility than weld 020 (Fig. 19D), though still low as expected for a lap joint weld. The tensile tested specimens (Fig. 20E) again show failure outside the fusion zone. Since failure is through the lower sheet, the tensile strength can be calculated based on the thickness (1.6 mm) of the lower sheet. The joint strength is 67% of the base metal strength. Again, the joint strength is expected to be lower for lap joint welds than butt joint welds. It can be seen from welds 018, 020, and 031 that lap joint welds without fingers tend to have higher ductility.

Conclusions

The following conclusions can be drawn based on the results from the butt and lap joint welding of AZ31 Mg sheets by CSC-GMAW:

1) Sound butt joint welds of Mg alloy sheets can be made by CSC-GMAW without spatter and hydrogen porosity, and they can approach 100% of the base metal strength.

2) However, precautions need be taken to avoid the formation of: 1) entrapped oxide films inside butt joint welds, 2) high crowns on butt joint welds, and 3) fingers from lap joint welds. These defects are caused mainly by the unusual physical and chemical properties of Mg rather than the welding process itself. Weld tensile specimens containing one or more of these defects are consistently found to fail at a significantly lower elongation.

3) The mechanism for oxide-film entrapment is as follows: The as-sheared edges of Mg sheets are rough (due to the poor deformability of Mg associated with its hcp structure), and they can form an air channel to cause the faying surfaces ahead of the weld pool to oxidize (due to the very high oxygen affinity of Mg), and the oxide films and air bubbles entrapped in the weld pool cannot rise quickly to escape (due to the low density of Mg).

4) A folded oxide film, called a bifilm, can form essentially along the central plane of the fusion zone and provide a very sharp notch to initiate crack under tension, leading to premature failure.

5) Milling the rough as-sheared edges of Mg sheets to make them smooth or providing an opening between the as-sheared faying surfaces can help eliminate the entrapment of oxide films and air bubbles.

6) The mechanism for the formation of high crowns is as follows: The low fluidity of Mg makes the weld pool solidify quickly before spreading out significantly to reduce the pool height. The low fluidity is caused mainly by the low density and hence low volumetric heat content of Mg, but it can be further reduced by the short-circuiting mode of metal transfer, including that in CSC-GMAW.

7) Widening the root opening can

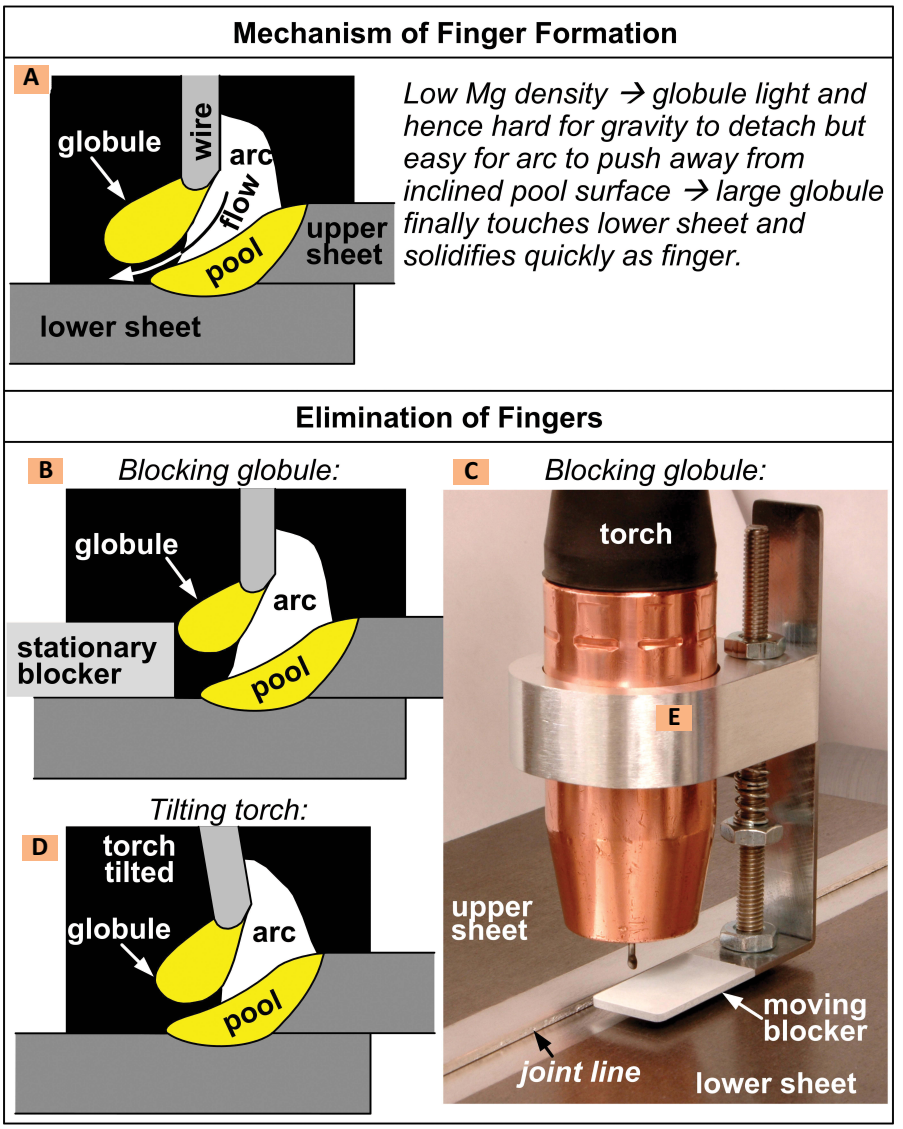

Fig. 18 — Mechanism and elimination of finger formation. A — Mechanism; B — eliminating fingers with stationary blocker; C — eliminating fingers with moving blocker; D — eliminating fingers by torch tilting.

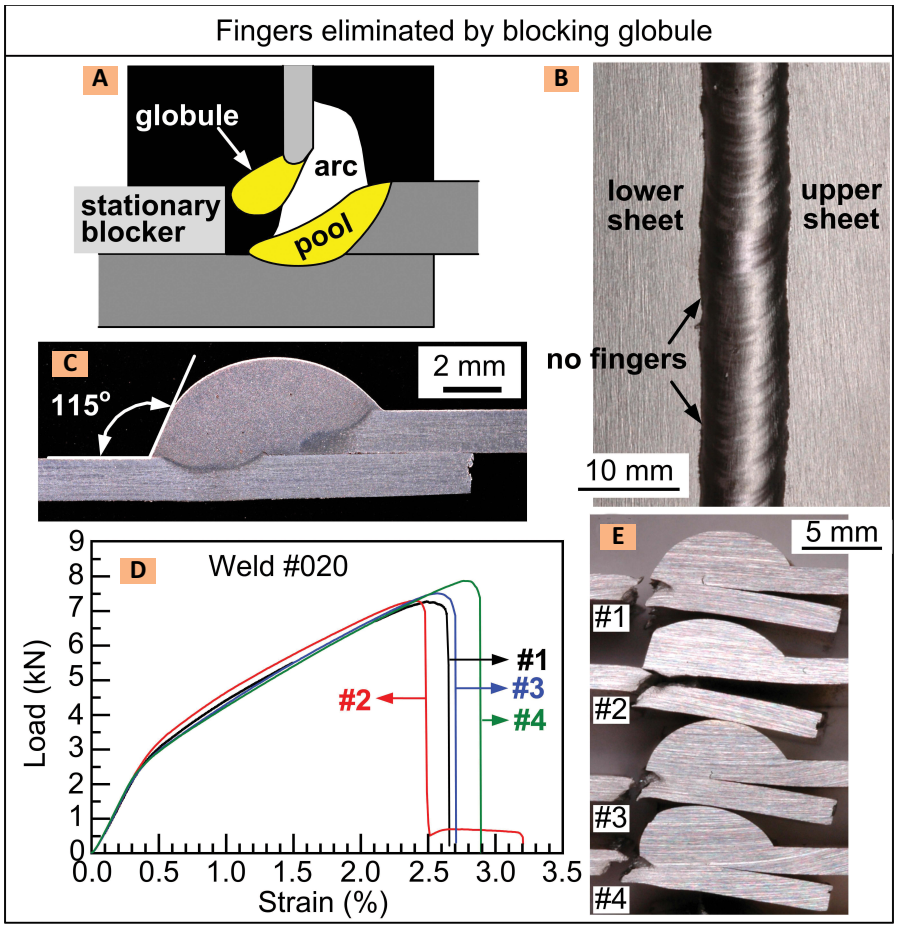

Fig. 19 — Elimination of fingers from lap weld 020 by blocking the globule. A — stationary blocker in the form of a BN-coated steel bar resting on lower sheet parallel to welding direction; B — top view of weld showing no fingers; C— transverse cross-section; D — tensile test curves; E — side views of tensile-tested specimens showing failure outside, instead of through, fusion zone (unlike weld 018 in Fig. 17).

help reduce the crown height by letting the liquid filler metal pass through quickly before solidification and providing extra space to accommodate the filler metal deposit. Deepening the groove in the backing plate can also help reduce the crown height by providing extra space to accommodate the filler metal deposit.

8) The mechanism for the formation of fingers is as follows: The low Mg density makes the filler metal globule light and hence difficult for gravity to detach it but easy for the arc jet to push it away from the inclined pool surface toward the lower sheet. The globule keeps growing and eventually touches the lower sheet to solidify on it quickly as a finger.

9) Using a piece of inert material (such as BN-coated steel) to block the globule can help eliminate fingers. The piece can either rest on the lower sheet or travel with the welding gun. Tilting the welding gun to shift the globule toward the upper sheet can also help eliminate fingers.

Acknowledgments

This work was supported by initially by General Motors and subsequently by the National Science Foundation under Grant No. IIP-1034695, the American Welding Society Foundation Fellowship Program, and the University of Wisconsin Foundation through the Industry/University Collaborative Research Center (I/UCRC) for Integrated Materials Joining Science for Energy Applications.

The author Sindo Kou would like to express his sincere thanks to Drs. Jim Yen-lung Chen and Xiaohong Q. Gayden of General Motors for getting GM's approval to support the project on GMAW welding of Mg alloys.

The authors would also like to thank Bruce Albrecht, Todd Holverson, Rick Hutchison, and Joe Fink of Miller Electric Manufacturing Co. and ITW Global Welding Technology Center, both located in Appleton, Wis., for donating the CSC process controller and drive assembly, Invision 456 power source, XR-M wire feeder, and welding gun used in the study.

References

1. Watarai, H. 2006. Trend of research and development for magnesium alloys — Reducing the weight of structural materials in motor vehicles. *Quarterly Review* 18: 84–97.

2. Magnesium Vision 2020: A North American automotive strategic vision for magnesium. USAMP, United States Automotive Materials Partnership – a consortium of the United States Council for Automotive Research, MG 2020, released 11/1/2006, pp. 1–34.

3. Kulekci, M. K. 2008. Magnesium and its alloys applications in automotive industry. *International Journal of Advanced Manufacturing Technology* 39: 851–865.

4. Feng, J., Wang, Y., and Zhang, Z. 2005. Status and expectation of research on welding of magnesium alloys. *The Chinese Journal of Nonferrous Metals* 15(2): 165–178 (in Chinese).

5. Deinzer, G. H., and Rethmeier, M. 2006. *Magnesium Technology — Metallurgy, Design Data and Applications*. H. E. Friedrich and B. L. Mordike, pp. 349–363, Verlag, Springer.

6. Cao, X., Jahazi, M., Immarigeon, J. P., and Wallace, W. 2006. A review of laser welding techniques for magnesium alloys. *Journal of Materials Processing Technology* 171: 188–204.

7. Liu, L. 2012. *Welding and Joining of Magnesium Alloys*. Cambridge, UK, Woodhead Publishing.

8. 1997. O'Brien, R. L. *Jefferson's Welding Encyclopedia*, 18th edition, American Welding Society, Miami, Fla., p. 484.

9. Rethmeier, M., Kleinpeter, B., and Wohlfahrt, H. 2004. MIG welding of magnesium alloys metallographic aspects. *Welding in the World* 48(3/4): 28–33.

10. Lockwood, L. F. 1963. Gas metal arc welding of AZ31B magnesium alloy sheet. *Welding Journal* 42: 807–818.

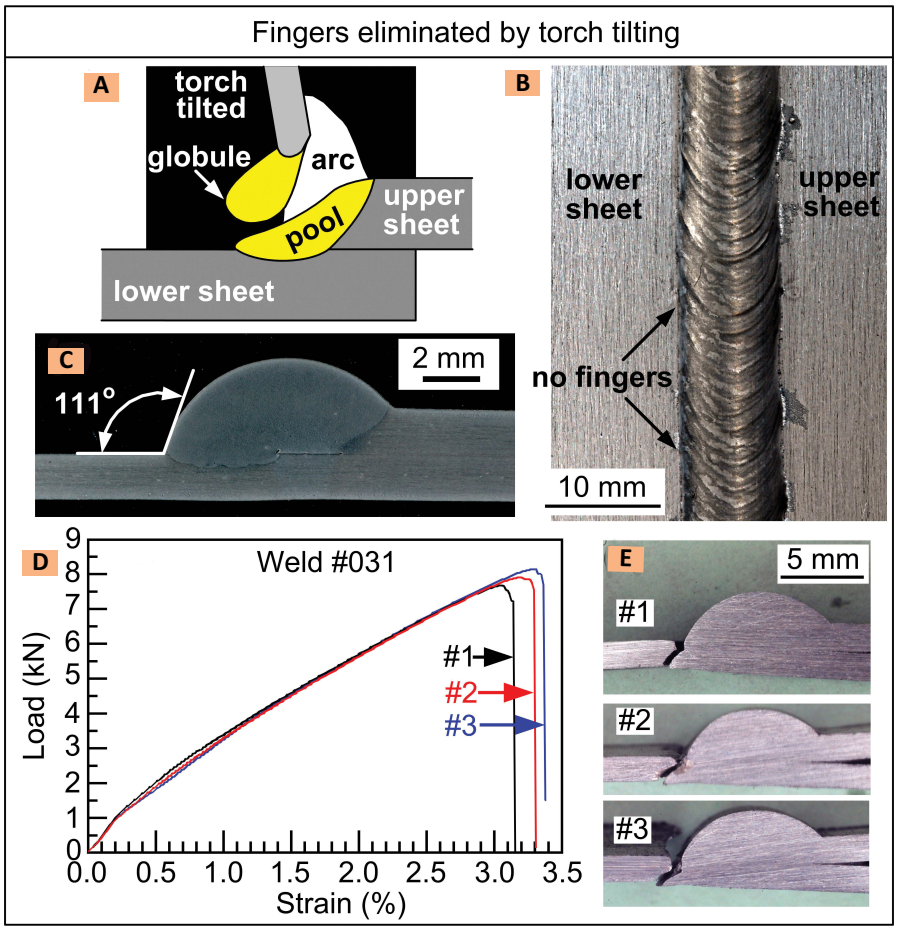

Fig. 20 — Elimination of fingers from lap weld 031 by welding gun tilting. A — Tilting the welding gun and hence the welding wire slightly toward the upper piece; B — top view of weld; C — transverse cross section; D — tensile test curves; E — side views of tensile-tested specimens showing specimens failed outside, instead of through, fusion zone (unlike weld 018 in Fig. 17).

11. Lockwood, L. F. 1970. Pulse-arc welding of magnesium. *Welding Journal* 49: 464–475.

12. Rethmeier, M., Wiesner, S., and Wohlfahrt, H. 2000. Influences on the static and dynamic strength of MIG-welded magnesium alloys. *Magnesium Alloys and Their Applications*, Wiley-VCH Verlag GmbH, pp. 200–204.

13. Marya, M., Edwards, G. R., and Liu, S. 2004. An investigation on the effects of gases in GTA welding of a wrought AZ80 magnesium alloy. *Welding Journal* 83: 203-s to 214-s.

14. Zhao, H., and DebRoy, T. 2001. Pore formation during laser beam welding of die-cast magnesium alloy AM60B — Mechanism and remedy. *Welding Journal* 80: 204-s to 210-s.

15. Chi, C.-T., Chao, C.-G., Liu, T.-F., and Wang, C.-C. 2008. Optimal parameters for low and high voltage electron beam welding of AZ series magnesium alloys and mechanism of weld shape and pore formation. *Science and Technology of Welding and Joining* 13(2): 199–211.

16. Park, S. H. C., Sato, Y. S., and Kokawa, H. 2003. Microstructural evolution and its effect of Hall-Petch relationship in friction stir welding of thixomolded Mg alloy AZ91D. *Journal of Materials Science* 38: 4379–4383.

17. Chowdhury, S. M., Chen, D. L., Bhole, S. D., Cao, X., Powidajko, E., Weckman, D. C., and Zhou, Y. 2010. Tensile properties and strain-hardening behavior of double-sided arc welded and friction stir welded AZ31B magnesium alloy. *Materials Science and Engineering A* 527: 2951–2961.

18. Wagner, D. C., Yang, Y. K., and Kou, S. 2013. Spatter and porosity in gas-metal arc welding of magnesium alloys: Mechanisms and elimination. *Welding Journal* 92: 347-s to 362-s.

19. CSC-MIG Weld Process Controller. Jetline Engineering, Irvine, Calif. *http://pdf.directindustry.com/pdf/jet-line-engineering/csc-mig-weld-process-controller/27577-54392.html*.

20. Kou, S. 2003. *Welding Metallurgy, 2nd edition*. pp. 122–141, 97–121, and 301–340, Hoboken, N. J., John Wiley & Sons.

21. Song, G., Wang, P., and Liu, L. M. 2010. Study on arc welding of AZ31B magnesium alloy. *Science and Technology of Welding and Joining* 15(3): 219–225.

22. Prasad, K. E., Li, B., Dixit, N., Shaffer, M., Mathaudhu, S. N., and Ramesh, K. T. 2014. The dynamic flow and failure behavior of magnesium and magnesium alloys. *JOM* 66(2): 291–304.

23. Darken, L. S., and Gurry, R. W. 1953. *Physical Chemistry of Metals*, p. 349. New York, McGraw-Hill.

24. Campbell, J. 2003. *Castings,* 2nd edition. pp. 17–69, Oxford, UK, Butter-Worth Heinemann.

25. Coniglio, N., and Cross, C. E. 2009. Mechanisms for solidification crack initiation and growth in aluminum welding. *Metallurgical and Materials Transaction A* 40A(11): 2718–2728.

26. Kou, S. 1996. *Transport Phenomena and Materials Processing*, pp. 499–514, Hoboken, N. J., John Wiley and Sons.

27. Laudise, R. A. 1970. *The Growth of Single Crystals*. pp. 201, 202, Englewood Cliffs, N. J., Prentice-Hall.

28. Iida, T., and Guthrie, R. I. L. 1988. *The Physical Properties of Liquid Metals*. p. 134, Oxford University Press.

29. *Thermal Conductivity — Theory, Properties, and Applications*. 2004. Edited by T. M. Tritt, pp. 28, 29. New York, Kluwer Academic/Plenum Publishers.

30. *Metals Handbook*. 9th ed., Vol. 2, pp. 714, 764, Metals Park, Ohio: ASM International.

31. Flemings, M. C. 1974. *Solidification Processing*. p. 14, New York, N.Y., McGraw-Hill.

AWS Peer Review Panel

All papers published in the *Welding Journal*'s Welding Research Supplement undergo Peer Review before publication for: 1) originality of the contribution; 2) technical value to the welding community; 3) prior publication of the material being reviewed; 4) proper credit to others working in the same area; and 5) justification of the conclusions, based on the work performed. The following individuals serve on the AWS Peer Review Panel and are experts in specific technical areas. All are volunteers in the program.

D. K. Aidun
M. C. Akuner
A. AlShawaf
T. Anderson
J. Antonini
A. Arora
K. D. Ashtekar
R. E. Avery
N. K. Babu
S. Bag
D. Bechetti
A. M. Beese
M. Bloss
S. Boetcher
J. E. M. Braid
R. Branan
J. Brauser
K. L. Brown
B. Brust
D. W. Bucholz
G. Buffa
D. Burford
P. Burgardt
X. Cao
Y. Chai
S. Chakraborty
C. L. Chan
K. R. Chan
B. Y. J. Chao
C. C. Chen
J. Chen
J. Chen
M. J. Cola
K. Colligan
G. E. Cook
B. Craig
M. Cunningham
E. N. C. Dalder
B. K. Damkroger
P. Dawson
L. De Filippis
A. Debiccari
B. DeForce
P. J. Ditzel
H. Dong
H. Doude
W. Drake
D. Dunbar
M. Dutoit
P. Dutta
C. Emmelmann
D. Eno
R. Etien
Z. Fang
J. D. Farren
D. A. Fink
S. R. Fiore
K. Friis
J. Gabbita
P. Gadhe
G. W. Galanes
W. F. Gale
D. L. Galiher
Y. P. Gao
J. A. Gianetto
B. Girvin
S. Gordon
K. Graff
M. Gray
J. Greer
M. Guhel
M. Hackett
P. Hall
M. Hanson
I. D. Harris
D. Hauser
V. B. Hernandez
G. Hinkle
K. Hollis
T. Hong
S. Horikawa
B. Horn
W. Hou
A. Hu
J. Hu
Y. Huang
J. Hutchins
D. L. Isenhour
J. R. Jachna
D. A. Javernick
N. T. Jenkins
C. Jiang
M. Q. Johnson
J. E. Jones
A. Kar
L. Karlsson
A. Kasapoğlu
S. Katayama
D. D. Kautz
F. Kavanara
S. C. Kelley
C. Kelly
S. Kelly
R. K. Kersey
I. Khan
D. S. Kim
J. K. Kim
Y. S. Kim
M. Kimchi
D. Klingman
D. B. Knorr
H. Koike
F. Kong
S. Kore
T. Kostrivas
R. Kovacevic
L. Kramer
A. Kumar
M. Kuntz
L. Kvidahl
J. J. Kwiatkowski
M. Labbe
K. Lachenberg
C. R. LaMorte
A. Landau
B. Leister
L. Li
M. V. Li
T. Li
W. Li
D. Liang
S. Lillard
Y. Liu
C. C. Lu
W. Lu
Y. Lu
D. Ludwig
N. Ma
X. Ma
D. Maatz
D. MacCallum
M. Manohar
I. Maroef
B. Marschke
F. Martinez Diez
R. P. Martukanitz
M. P. Marya
S. Massey
K. Masubuchi
V. Matthews
M. Mayer
A. Maynard
J. Mazumder
M. McAninch
S. McCracken
A. McDonald
A. Mengel
R. Menon
M. P. Miles
J. O. Milewski
D. Miller
R. Mishra
T. Morrissett
P. E. Murray
S. J. Na
X. Na
B. Narayanan
A. M. Nasiri
T. V. Natale
T. C. Nguyen
M. Nicas
N. E. Nissley
J. T. Norris
Y. Ogawa
T. Oyama
A. Pandey
J. Peng
J. A. Penso
F. Perez
E. C. Pessoa
W. Peterson
C. Pettersson
A. Peusc
F. Pfefferkorn
S. Pilli
M. Piltch
J. P. Planckaert
A. Polar
N. Porter
M. Prager
P. Prangnell
M. Prime
J. D. Puskar
J. Querin
T. P. Quinn
A. Rabinkin
J. Ram
A. Raraz
S. Ream
C. B. Reed
R. Ress
A. P. Reynolds
D. Richards
B. Ridgway
J. R. Roper
G. Roy
D. Rudland
F. Rumiche
D. J. Rybicki
E. F. Rybicki
S. Sadagopan
S. Santhanakrishnan
D. Schick
J. Scott
K. Scott
O. Semenov
D. Sen
A. Shapiro
A. Shukla
M. Siddens
M. S. Sierdzinski
T. Siewert
M. Sinfield
D. Sirois
H. B. Smartt
C. Smith
B. R. Somers
R. Somers
H. Song
W. H. Song
G. Sonnenberg
C. D. Sorensen
V. Soundararajan
W. J. Sperko
J. E. Stallmeyer
R. J. Steele
A. W. Stockdale
R. T. Stone
T. Stotler
J. Sutliff
E. Taban
H. Tang
M. Teague
K. Tello
D. J. Tillack
W. Tong
D. W. Trees
C. L. Tsai
J. Tucker
G. D. Uttrachi
D. M. Vandergriff
P. T. Vianco
B. Victor
C. A. Walker
G. Wang
H. P. Wang
W. Wang
Y. Y. Wang
R. Warke
D. C. Weckman
P. S. Wei
M. M. Weir
E. M. Westin
T. C. Wheeler
T. Wong
P. Woollin
C. Wu
C. Y. Wu
L. Xiao
J. Xie
P. P. Xu
R. Xu
S. Xu
Z. Xu
Z. Yang
L. Yepez
G. Young
X. Yu
C. Zhang
P. Zhang
R. Zhang
W. Zhang

Principal Reviewers

Y. Adonyi
B. Alexandrov
S. S. Babu
M. Balmforth
D. Barborak
J. L. Caron
H. R. Castner
B. A. Chin
C. E. Cross
C. B. Dallam
T. DebRoy
X. Deng
J. N. DuPont
T. W. Eagar
J. W. Elmer
D. F. Farson
Z. Feng
R. W. Fonda
P. W. Fuerschbach
A. Gerlich
J. E. Gould
M. Harris
D. Hartman
T. Hitchcock
P. Hochanadel
T. Holverson
F. M. Hosking
Y. Huang
R. Hutchison
J. E. Indacochea
G. A. Knorovsky
P. J. Konkol
D. J. Kotecki
S. Kou
S. H. La Lam
D. Landon
K. Li
L. Li
T. W. Liao
T. J. Lienert
D. Lin
W. Lin
S. Liu
W. Liu
R. B. Madigan
M. C. Maguire
P. F. Mendez
D. W. Meyer
P. Michaleris
W. Mohr
P. B. Nagy
R. Nandan
T. W. Nelson
R. Noecker
D. L. Olson
T. A. Palmer
J. J. Perdomo
M. J. Perricone
R. Polanin
M. Posada
A. J. Ramirez
J. Ramirez
G. W. Ritter
J. Rodelas
J. Schneider
D. R. Sigler
X. Sun
D. Susan
M. Tumuluru
P. C. Wang
Y. P. Yang
Z. Yu
H. Zhang
W. Zhang
Y. M. Zhang
Y. N. Zhou